spectroscopy (JEOL JNM-EX 500 MHz) and elemental analysis (Perkin–Elmer 2400II CHNS/O).

2.2.1. N,N′-Dialkylethylenediamine: (n)-2-(n)

Ethylenediamine (0.25 mol) was firstly mixed with 50 cm^3 of 1-propanol, and then 1-bromoalkane (0.53 mol) was added dropwise to this mixture under a mild alkaline condition with methanol NaOH solution. The reaction system was then refluxed for 24 h. The mixture was filtered under hot conditions to remove insoluble salts. After the filtrate was evaporated, the residue was poured in an aqueous NaOH solution (pH ~13.5) and was stirred for 6 h. White products were obtained, after filtration of the aqueous mixture and subsequent drying in a desiccator. The white products were again dissolved in 800 cm^3 of diethylether and then HCl gas was introduced into this solution. After filtration of the crystalline white products from the diethylether solution, recrystallization was performed three times using either ethanol (for $n = 8$ and 10) or a mixed solvent of ethanol containing a small amount of methanol (for $n = 12$). The yield was approximately 50% for all the analogues at this stage.

The white products were poured into deionized water at pH 13.5 (adjusted with NaOH) and then the aqueous solution was boiled under stirring. As the solution was cooled down to room temperature, white products were seen in the bottom of the reaction vessel. This boiling-cooling procedure was repeated three times. Then the solution was extracted with diethylether. This diethylether solution was cooled down to 0 °C with ice and was recrystallized. After filtration and subsequent drying in a desiccator, the obtained white products were again recrystallized with dried acetone three times. The products obtained here were white and needle-like crystal. The yield was approximately 50% for all the products.

^{1}H NMR (CD_3OD): δ 0.88–0.91 (t, 6H, $2CH_3$–CH_2–), 1.28–1.32 (m, $4(n-3)$H, $2CH_3$–$(CH_2)_{n-3}$–CH_2–), 1.50–1.53 (m, 4H, 2–$(CH_2)_{n-3}$–CH_2–CH_2–), 2.57–2.60 (t, 4H, 2–CH_2–CH_2–N–), 2.72 ppm (s, 4H, –CH_2–N(–CO–)–CH_2–CH_2–N(–CO–)–CH_2–).

Elemental analysis: *(8)-2-(8)* calculated for $C_{18}H_{40}N_2 \cdot 1H_2O$: C, 71.46; H, 13.99; N, 9.26. Found: C, 71.44; H, 13.66; N, 9.28. *(10)-2-(10)* calculated for $C_{22}H_{48}N_2 \cdot 1H_2O$: C, 73.68; H, 14.05; N, 7.81. Found: C, 73.95; H, 14.55; N, 7.90. *(12)-2-(12)* calculated for $C_{26}H_{56}N_2 \cdot 1H_2O$: C, 75.29; H, 14.10; N, 6.75. Found: C, 75.59; H, 14.13; N, 6.80.

2.2.2. N,N′-Dialkyl-N,N′-digluconamide ethylenediamine: Glu(n)-2-Glu(n)

D-(+)-Glucono-1,5-lactone (ca. 0.039–0.054 mol) was added to a methanol solution (100 cm^3) of (*n*)-2-(*n*) (5 g, ca. 0.013–0.018 mol). The mixture was stirred for 1 week at room temperature (approximately 25 °C), refluxed for 3 h and then evaporated. The obtained residue was washed with hexane three times to remove un-reacted (*n*)-2-(*n*). After this washing, the products were dissolved in dried acetone. The solution was stirred for 24 h and then centrifuged in order to remove some insoluble impurities. The residue, obtained with evaporation from acetone, was dried in a desiccator. In a similar way to this procedure, the products were washed with dried ethanol three times, and finally, they were recrystallized from a mixed solvent of dried acetonitrile containing a small amount of ethanol. The final products were phlegmatic and the yield was 9–19%.

^{1}H NMR (CD_3OD): δ 0.88–0.91 (t, 6H, $2CH_3$–CH_2–), 1.27–1.35 (m, $4(n-3)$H, $2CH_3$–$(CH_2)_{n-3}$–CH_2–), 1.60–1.65 (m, 4H, 2–$(CH_2)_{n-3}$–CH_2–CH_2–), 3.35–3.50 (m, 8H, 2–CH_2–N–, –CH_2–N(–CO–)–CH_2–CH_2–N(–CO–)–CH_2–), 3.60–4.30 ppm (m, 12H, protons from sugar moieties).

Elemental analysis: *Glu(8)-2-Glu(8)* calculated for $C_{30}H_{60}N_2O_{12}$: C, 52.27; H, 8.35; N, 2.90. Found: C, 52.41; H, 8.27; N, 2.89. *Glu(10)-2-Glu(10)* calculated for $C_{34}H_{68}N_2O_{12}$: C, 54.10; H, 8.69; N, 2.74. Found: C, 54.36; H, 9.07; N, 2.78. *Glu(12)-2-Glu(12)* calculated for $C_{38}H_{76}N_2O_{12}$: C, 55.74; H, 8.98; N, 2.60. Found: C, 55.38; H, 8.63; N, 2.54.

2.3. Measurements

The aqueous surfactant solutions were prepared via direct dissolution of the phlegmatic samples at the desired concentration. For all the surfactants used in this work, no precipitation or phase separation was seen in a whole range of the concentration investigated. All measurements reported here were performed at 25 °C.

The static surface tension was measured using a Kyowa Wilhelmy auto surface tensiometer CBVP-Z with a platinum plate. Note that the measurements were continuously carried out until a change in the surface tension becomes less than 0.1 mN m^{-1} per 15 min. The dynamic surface tension (γ_t) was estimated using a Krüss BP2 MK2 bubble pressure tensiometer, applying the following equation:

$$\gamma_t = (P_{max} - P_0) \times \frac{r}{2}, \quad (1)$$

where P_{max} is the maximum bubble pressure at the air/aqueous solution interface, P_0 is the pressure measured in a capillary for the air/pure water interface and r is the radius of the capillary interior. The measurements were conducted with effective surface ages from 5 ms to 30 s.

In order to estimate the micro-environmental polarity of the micelle interiors, steady-state fluorescence measurements were performed using a Shimazu RF-5300PC fluorescence spectrophotometer. The spectrum was recorded between 360 and 400 nm with the excitation wavelength of 335 nm. The concentration of pyrene as a fluorescence probe was set to approximately 1 μmol dm^{-3}. As well known [25,26], the fluorescence intensity ratio of the first (373 nm) to the third (384 nm) vibrational peaks (I_1/I_3) indicates the micro-environmental polarity around the pyrene molecules: the decrease in the I_1/I_3 value is indicative of the formation of the more hydrophobic environments.

The hydrodynamic diameter of the surfactant micelles in the solution phase was estimated using an IBC NICOMP 380ZLS particle size analyzer equipped with a 5 mW He–Ne laser at a constant detector angle of 90°. The obtained scattering data were fitted using an intensity-weighted cumulative analysis to

estimate the diffusion coefficient of the surfactant micelles in aqueous solution. The hydrodynamic diameter of the micelles was obtained from the diffusion coefficient using the Stokes–Einstein equation [27]. All sample solutions were filtered with a 0.2 μm cellulose acetate membrane filter before measurements.

For cryo-TEM measurements, the sample grid was prepared as follows: (i) a small amount of sample solution was mounted on a TEM cupper grid coated with a holey carbon film; (ii) the grid was mounted by a pair of self-locking tweezers; (iii) the excess amount of the sample solution was removed from the grid using a filter paper; and finally (iv) the grid was introduced into liquid ethane cooled by liquid nitrogen. The prepared grid was then set on the cryo-specimen holder under liquid nitrogen cooling. Cryo-TEM measurements were made using a Hitachi H-7650 at an accelerating voltage of 120 kV under a low electron dose.

3. Results and discussion

3.1. Adsorption to the air/aqueous solution interface

Fig. 2 shows the static surface tension of aqueous solutions of Glu(n)-2-Glu(n) (n = 8, 10 and 12) as a function of the concentration. The equilibrium surface tension values were obtained within 3–6 h in the higher concentration region, whereas the longer equilibration time (approximately 20–30 h) was required in the lower concentration region. The equilibration time was also dependent on the hydrocarbon chain length and an increase in the chain length results in the longer time to reach the equilibrium (see also dynamic surface tension data).

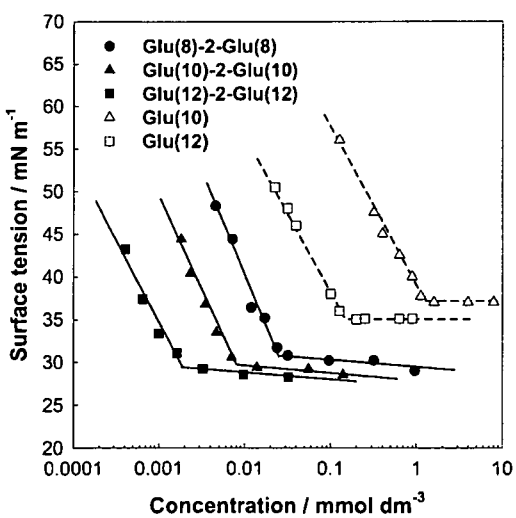

Fig. 2. Static surface tension of aqueous Glu(n)-2-Glu(n) (n = 8, 10 and 12) solutions as a function of the concentration. Also shown are the corresponding data of Glu(n) (n = 10 and 12), reported in the previous paper [6].

In the region of low surfactant concentrations the surface tension decreases sharply with increasing concentration and attains a break point. The surfactant concentration attained to this break point is assumed to be the cmc of each surfactant. Interestingly, a gradual decrease in the surface tension is observed even when the surfactant concentration exceeds the cmc. Such a decrease in the surface tension has similarly been observed for a number of other gemini surfactants [28,29], although the exact reason has not been presented. We infer that the decrease in the surface tension observed above the cmc of Glu(n)-2-Glu(n) results from the formation of a closely packed monolayer film of the gemini surfactants, caused by the further adsorption of the surfactants to the air/aqueous solution interface. This may be rationalized when admitting the fact that the gemini surfactants adsorbed at the interface are molecularly squeezable due to the presence of the spacer chain (and relatively small headgroups), and thereby, the further adsorption sites are provided even above the cmc. Also given in Fig. 2 are the surface tension data of the corresponding monomeric surfactants, Glu(n) (n = 10 and 12), reported previously [6]. Apparently, the values of the surface tension measured above the cmc are almost constant for these monomeric surfactants.

The surface tension data shown in Fig. 2 allow us to calculate some physicochemical parameters (see Table 1): the surface excess concentration estimated at the cmc (Γ_{cmc}), the occupied area per molecule at the cmc (A_{cmc}), the standard free energy of micellization that occurs in bulk solution (ΔG^0_{mic}) and the standard free energy of adsorption to the air/aqueous solution interface (ΔG^0_{ads}) [30],

$$\Gamma_{cmc} = -\frac{1}{RT}\frac{d\gamma}{d\ln C}, \tag{2}$$

$$A_{cmc} = \frac{1}{N_A \Gamma_{cmc}}, \tag{3}$$

$$\Delta G^0_{mic} = RT \ln\left(\frac{cmc}{\omega}\right), \tag{4}$$

$$\Delta G^0_{ads} = \Delta G^0_{mic} - \left(\frac{\gamma_0 - \gamma_{cmc}}{\Gamma_{cmc}}\right), \tag{5}$$

where γ is the equilibrium surface tension measured at the surfactant concentration of C, γ_0 is the surface tension of pure water, ω is the molarity of water, T is the absolute tempera-

Table 1
Physicochemical properties of sugar-based monomeric and gemini surfactants on the basis of static surface tension data

	cmc (mmol dm^{-3})	γ_{cmc} (mN m^{-1})	Γ_{cmc} (μmol m^{-2})	A_{cmc} (nm^2 mol^{-1})	ΔG^0_{mic} (kJ mol^{-1})	ΔG^0_{ads} (kJ mol^{-1})	pC_{20}
Glu(8)-2-Glu(8)	0.0268	30.7	3.89	0.428	−36.1	−46.7	5.53
Glu(10)-2-Glu(10)	0.00655	30.3	3.99	0.412	−39.6	−50.0	6.14
Glu(12)-2-Glu(12)	0.00146	29.6	4.14	0.402	−43.3	−53.5	6.79
Glu(10)[a]	1.29	35.9	3.96	0.420	−16.2	−20.2	3.60
Glu(12)[a]	0.146	34.4	3.99	0.420	−21.5	−26.8	4.78

[a] From Ref. [6].

ture, N_A is the Avogadro's number and R is the gas constant. We also calculated the pC_{20} value of each surfactant: the C_{20} value is defined to be the surfactant concentration where a decrease in the surface tension of 20 mN m^{-1} from pure water is recorded ($pC_{20} = -\log C_{20}$), and therefore, this value is indicative of an efficiency in lowering the surface tension [30]. For the Glu(n)-2-Glu(n) surfactants, the increase in the hydrocarbon chain length results in (i) a significant decrease in the cmc (in a similar way observed for the monomeric Glu(n) surfactants), (ii) an increase in the pC_{20} and (iii) an increase in the absolute value of the ΔG^0_{ads}. The combination of these results suggests that the adsorption of the Glu(n)-2-Glu(n) surfactants to the air/aqueous solution interface occurs more effectively for the longer chain analogue than for the shorter one, as a result of the greater hydrophobic character of the longer chain analogue. This necessarily leads to the formation of a closely packed monolayer film of the longer chain analogue at the air/aqueous solution interface, which is supported by the greater Γ_{cmc} value (and thereby, the smaller A_{cmc} value) of the longer chain analogue. We also note here that the calculated ΔG^0_{ads} value of the Glu(n)-2-Glu(n) surfactants is always negatively larger than the corresponding ΔG^0_{mic} value, indicating that the adsorption occurs predominantly over the micellization that is seen in aqueous solution. Such a predominance of adsorption has similarly been reported in the previous literatures focusing on the adsorption/micellization behavior of sugar-based gemini surfactants [14,23].

When compared with the data reported for the Glu(n) surfactants [6], one may notice that the cmc value of the Glu(n)-2-Glu(n) surfactants is observed to be approximately 100–200 times lower than that of the corresponding Glu(n) surfactants. This greater efficiency of the gemini surfactants in the adsorption/micellization is also supported by (i) the generally lower γ_{cmc}, (ii) the larger pC_{20} and (iii) the negatively larger ΔG^0_{ads} of the Glu(n)-2-Glu(n) surfactants. Interestingly, the occupied area of the Glu(n)-2-Glu(n) surfactants divided by the number of the hydrocarbon chain per molecule (i.e., 2) is found to be half of the occupied area of the corresponding Glu(n) surfactants. Again, this is reflective of the greater degree of the molecular packing of the Glu(n)-2-Glu(n) surfactants at the air/aqueous solution interface.

As noted in the Introduction, a series of glucono-lactone (monosaccharide) based nonionic gemini surfactants has been synthesized by Komorek and Wilk [14]. In accordance of their report, the gemini surfactant, consisting of two dodecyl chains linked with an ethylene spacer (i.e., corresponding to Glu(12)-2-Glu(12) in our current study), is able to lower the surface tension up to 32 mN m^{-1}, being comparable with the γ_{cmc} value recorded for the present Glu(12)-2-Glu(12) case. Nevertheless, the cmc and Γ_{cmc} values reported by the authors (cmc 3.8 μmol dm^{-3}; Γ_{cmc} 2.5 μmol m^{-2} [14]) differ significantly from the values of Glu(12)-2-Glu(12). Again, this results from the greater degree of molecular packing of Glu(12)-2-Glu(12) at the air/aqueous solution interface. The surfactant synthesized by the authors contains a propyl-peptide unit (i.e. –$CH_2CH_2CH_2$–NHCO–) between the sugar moiety and the tertiary amine group at the level of the ethylene spacer, and hence, the propyl-peptide unit may inhibit the closer packing when compared with the Glu(n)-2-Glu(n) surfactants used in our current study.

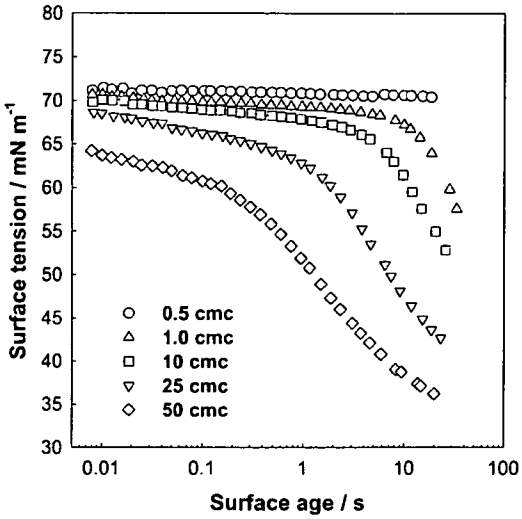

Fig. 3. Dynamic surface tension of aqueous Glu(8)-2-Glu(8) solutions with various concentrations.

The adsorption kinetics of the Glu(n)-2-Glu(n) surfactants to the air/aqueous solution interface have been studied on the basis of dynamic surface tension data. Fig. 3 shows the dynamic surface tension of Glu(8)-2-Glu(8), measured at the various concentrations. It is apparent from this figure that the observed decrease in the surface tension becomes faster as the surfactant concentration is increased, in a similar manner to that seen in our previous study [24]. We note that this phenomenon was similarly observed for all the surfactants used in the current study (data not shown).

In order to compare the adsorption kinetics of each Glu(n)-2-Glu(n) surfactant, the dynamic surface tension data recorded at a fixed concentration of 0.35 mmol dm^{-3} are plotted in Fig. 4. This concentration is well above the cmc of each gemini surfactant (see Table 1). It is known that adsorption kinetic data are analyzed by the following equation if the adsorption is controlled by the molecular diffusion of the adsorption species [31]:

$$\Gamma(t) = \sqrt{\frac{4D}{\pi}}\left(C_0 t^{1/2} + \int_0^t C_s(\tau)\, d\sqrt{t-\tau}\right), \tag{6}$$

where $\Gamma(t)$ is the surface excess concentration at time t, D is the apparent diffusion coefficient, C_0 is the concentration in bulk solution, $C_s(\tau)$ is the concentration at the sub-surface and τ is a dummy time-delay variable. In an attempt to bypass the need for complicated numerical solutions when analyzing the experimental data, asymptotic equations for both short- and long-time adsorption behaviors have been derived as follows [29,32–35]:

$$\text{short-time:}\quad \gamma(t) = \gamma_0 - 2C_0 RT\sqrt{\frac{Dt}{\pi}}, \tag{7}$$

$$\text{long-time:}\quad \gamma(t) = \gamma_{eq} + \frac{RT\Gamma_{eq}^2}{C_0}\sqrt{\frac{\pi}{4Dt}}, \tag{8}$$

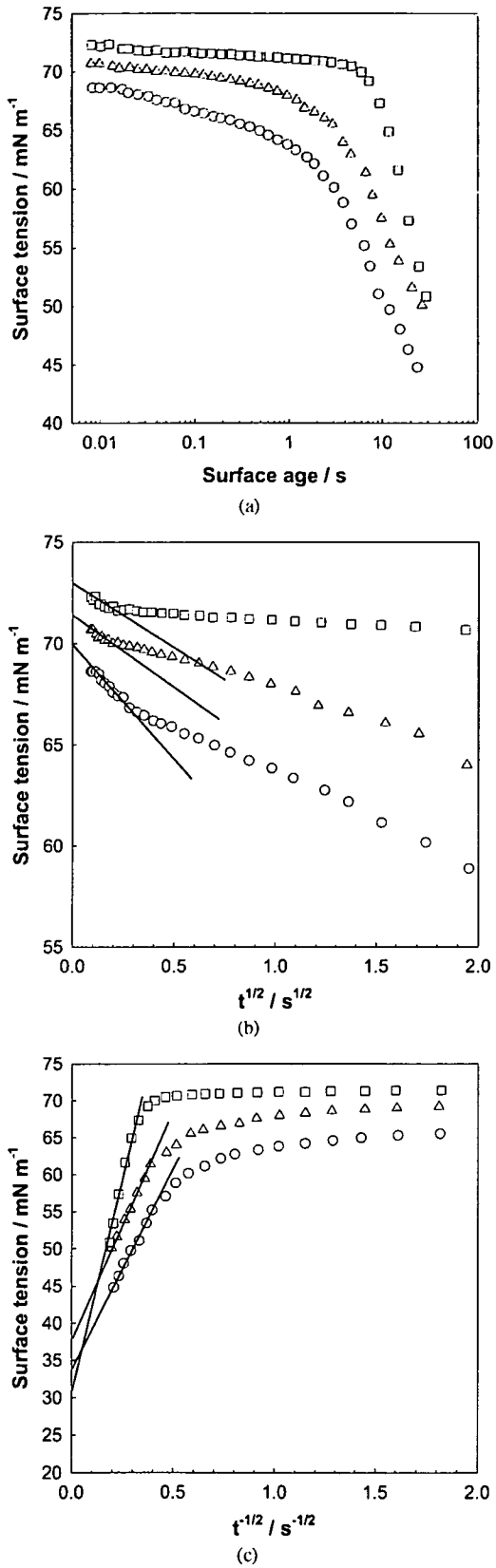

Fig. 4. Dynamic surface tension of aqueous Glu(n)-2-Glu(n) (n = 8 (○), 10 (△) and 12 (□)) solutions as a function of (a) the surface age t, (b) $t^{1/2}$ and (c) $t^{-1/2}$. The surfactant concentration is fixed at 0.35 mmol dm^{-3}.

Table 2
Apparent diffusion coefficients of Glu(n)-2-Glu(n) (at 0.35 mmol dm^{-3})

	D_{short} (m^2 s^{-1})	D_{long} (m^2 s^{-1})
Glu(8)-2-Glu(8)	1.5×10^{-10}	3.2×10^{-12}
Glu(10)-2-Glu(10)	3.9×10^{-11}	2.8×10^{-12}
Glu(12)-2-Glu(12)	1.7×10^{-11}	5.6×10^{-13}

where $\gamma(t)$ is the surface tension measured at time t. γ_{eq} is the equilibrium surface tension (at infinite time) and Γ_{eq} is the equilibrium surface excess concentration (to a first approximation, Γ_{eq} is assumed to be equal with Γ_{cmc}, estimated with static surface tension data). Equations (7) and (8) allow us to calculate the apparent diffusion coefficient from the slope of the dynamic surface tension data plots against $t^{1/2}$ (short-time, see Fig. 4b) or $t^{-1/2}$ (long-time, see Fig. 4c). The calculation results are summarized in Table 2. Both the diffusion coefficients estimated at the short-time (D_{short}) and long-time (D_{long}) decrease when the hydrocarbon chain length is increased. This suggests that the increase in the overall size of the surfactant molecules results in the decelerated rate of the interfacial adsorption. One possible interpretation for this is the more significant steric hindrance between the longer chain surfactants at the stage of molecular diffusion and/or subsequent rearrangement at the interface [36], although a difference in the cmc (and thereby, in the population of molecularly dissolved monomers in solution) may also make a significant impact on the adsorption kinetics.

3.2. Micellization in aqueous solution

Fig. 5 shows a change in the fluorescence intensity ratio (I_1/I_3) of pyrene as a function of the surfactant concentration. For the monomeric Glu(n) surfactants, the I_1/I_3 value starts to decrease from the cmc determined by the static surface tensiometry and the value attains a plateau level at the concentration well above the cmc. This is a typical trend for conventional monomeric surfactants and the micelle formation is suggested to occur in the bulk aqueous solution. Similarly, the I_1/I_3 value of the Glu(n)-2-Glu(n) surfactants starts to decrease when the surfactant concentration is increased to the cmc, however, the decrease in the I_1/I_3 is observed to be more gradual when compared with the data observed for the Glu(n) surfactants (this is particularly obvious in the cases of Glu(10)-2-Glu(10) and Glu(12)-2-Glu(12)). This means that the microenvironmental polarity of the Glu(n)-2-Glu(n) micelle core is gradually changed with increasing concentration. In order to understand such a difference in the micellization behavior for the monomeric and gemini surfactants, DLS and cryo-TEM measurements were performed.

The apparent hydrodynamic diameter of the Glu(n)-2-Glu(n) surfactant micelles, estimated from DLS measurements, is given in Fig. 6 as a function of the surfactant concentration. These diameter values were calculated under an assumption that the micelles are spherical. For the monomeric surfactants Glu(10) and Glu(12), the apparent hydrodynamic diameter is

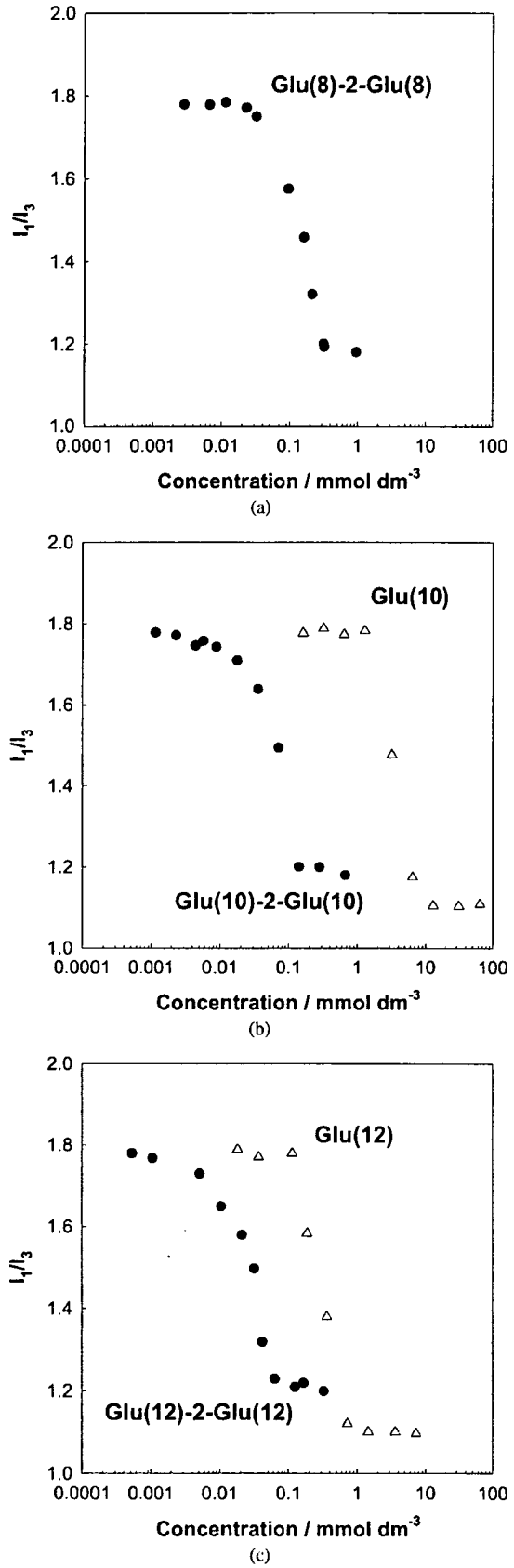

Fig. 5. Change in the fluorescence intensity ratio of pyrene as a function of the surfactant concentration: n = (a) 8, (b) 10 and (c) 12.

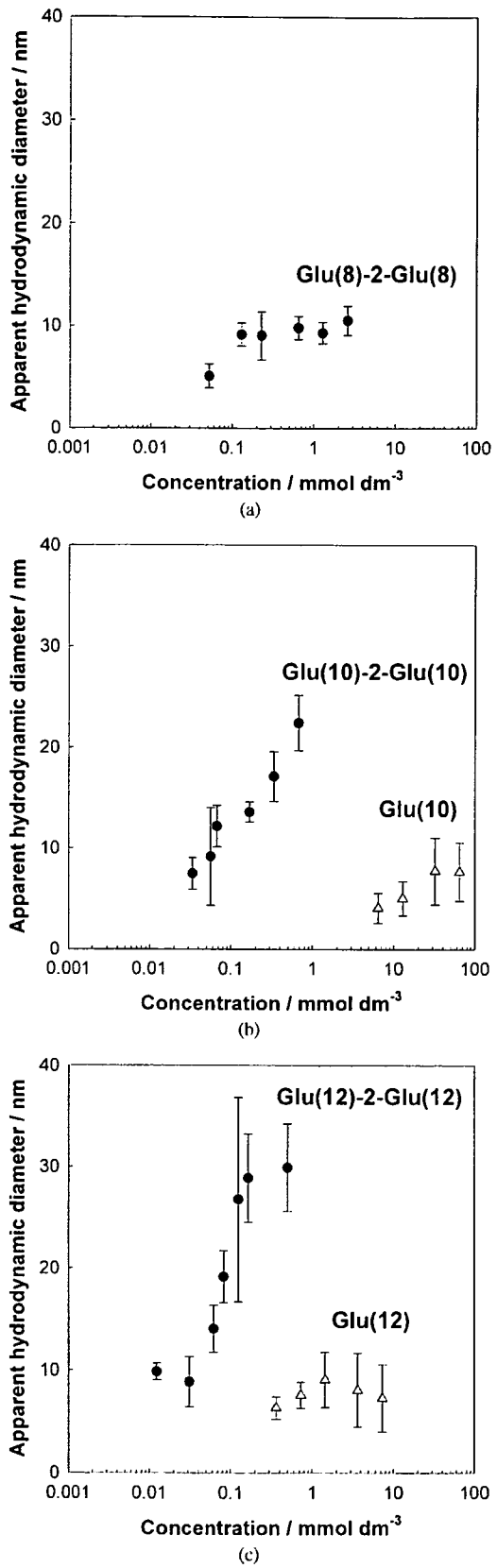

Fig. 6. Apparent hydrodynamic diameter of the Glu(n)-2-Glu(n) (n = 8, 10 and 12) and Glu(n) (n = 10 and 12) micelles as a function of the concentration: n = (a) 8, (b) 10 and (c) 12.

calculated to be 5–10 nm and a clear dependence on the surfactant concentration is not seen within the resolution of our experimental setup. For the gemini surfactants Glu(10)-2-Glu(10) and Glu(12)-2-Glu(12), on the other hand, a significant increase in the mean diameter is observed as the surfactant concentration is increased. Indeed, it seems that, for a given concentration, the hydrodynamic diameter of the Glu(n)-2-Glu(n) micelles increases with an increase in the hydrocarbon chain length. Clearly, the obtained DLS data suggest that a structural transformation of the Glu(n)-2-Glu(n) micelles takes place at the concentration above the cmc.

Cryo-TEM measurements were carried out for the Glu(n)-2-Glu(n) surfactants and a typical result of Glu(12)-2-Glu(12) is shown in Fig. 7. In this particular case the surfactant concentration is set to 0.5 mmol dm^{-3} (cmc ×350), where the relatively larger micelles are suggested to be formed on the basis of the DLS data. One can clearly see a worm-like micelle structure in Fig. 7. It was not possible to obtain a high-quality image just above the cmc, however, the increase in the apparent hydrodynamic diameter (see Fig. 6) may result from the formation of the worm-like micelles in aqueous solution. A reasonable interpretation for the formation of such worm-like micelles may lie in the theory of the surfactant packing parameter (SPP) [4]: gemini surfactants generally exhibit a larger SPP value when compared with monomeric surfactants, and therefore, rod-like or worm-like micellar aggregates are spontaneously formed even just above the cmc. This concept has been supported experimentally using a cationic gemini surfactant (dimethylene-1,2-bis(dodecyldimethylammonium bromide), 12-2-12), where a gradual sphere-to-cylinder transition of the micelle structure is reported with an increase in the concentration [37]. The formation of worm-like micelles has also been presented for the sugar-based gemini surfactant containing a tertiary amine linkage at the level of the hydrocarbon (hexyl) spacer, although the vesicle formation is observed to be more common (note that the worm-like structure is only seen under a mild acidic condition) [19]. According to the latter report, the vesicles formed at neutral pH are transformed into the worm-like micelles at lower pH values as a result of an increased electrostatic repulsion, caused by the protonation of the tertiary amine groups. Note that the surfactant used in the reported study contains oleyl (unsaturated C_{18}) chains as a hydrocarbon tail group. In addition, the glucono-lactone based headgroups of Glu(12)-2-Glu(12), concerning in the current study, are linked with the ethylene spacer via an amide linkage (instead of the direct linkage of the monosaccharide moieties with the tertiary amine groups), suggesting the larger head volume of Glu(12)-2-Glu(12). These differences in the chemical structure indicate the smaller SPP value of Glu(12)-2-Glu(12) when compared with the reported sugar-based gemini surfactant, and therefore, it is possible to rationalize that the worm-like micelles are spontaneously formed in the case of Glu(12)-2-Glu(12), as suggested by the present DLS and cryo-TEM data. Finally, we note that the 0.5 mmol dm^{-3} of Glu(12)-2-Glu(12) solution was found to be an Newtonian fluid on the basis of viscosity data (not shown). This finding is not always consistent with the cryo-TEM data, however, it seems likely that the surfactant concentration is not enough to provide any significant entanglements of the worm-like micelles in aqueous solution.

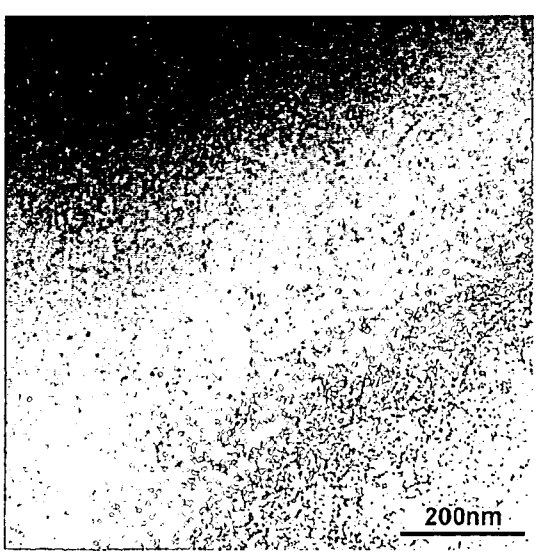

Fig. 7. A typical cryo-TEM image of Glu(12)-2-Glu(12) observed at 0.5 mmol dm^{-3} (cmc ×350).

4. Conclusions

The physicochemical properties of aqueous solutions of novel sugar-based gemini surfactants (Glu(n)-2-Glu(n)) have been presented. The monosaccharide headgroups of the surfactants are directly bound to the tertiary amine group at the level of an ethylene spacer. This means that the chemical structure of the gemini surfactants is molecularly restricted, and therefore, the surfactants are expected to be desirable for an excellent surface activity. In fact, it was found that, when compared to the corresponding monomeric surfactants, the gemini surfactants synthesized in the current study exhibit both (i) a greater ability in lowering the surface tension and (ii) a remarkably lower cmc. These phenomena are generally observed for a system of gemini surfactants, however, we emphasize that the ability in the adsorption and molecular association is more pronounced for the current Glu(n)-2-Glu(n) surfactants than for a similar type of sugar-based gemini surfactants synthesized previously in our group. This finding should be useful in developing high quality surfactants in a field of detergents and other consumer products.

The micellization behavior has been studied with a combination of the fluorescence, DLS and cryo-TEM data and it was suggested that, for all the Glu(n)-2-Glu(n) surfactants, a structural transformation occurs with increasing concentration. At the concentration well above the cmc, Glu(12)-2-Glu(12) spontaneously forms worm-like micelles, confirmed with cryo-TEM measurements. This is a unique feature of the Glu(n)-2-Glu(n) surfactants, because it is more usual to find worm-like morphology in either highly charged systems or in surfactant mixtures containing a co-surfactant.

References

[1] R. Zana, J. Xia (Eds.), Gemini Surfactants, Synthesis, Interfacial and Solution-Phase Behavior, and Applications, Marcel Dekker, New York, 2003, chap. 1.

[2] R. Zana, in: K. Esumi, M. Ueno (Eds.), Structure–Performance Relationships in Surfactants, second ed., Marcel Dekker, New York, 2003, chap. 7.

[3] R. Zana, E. Alami, in: K. Holmberg (Ed.), Novel Surfactants: Preparation, Applications, and Biodegradability, Marcel Dekker, New York, 2003, chap. 12.

[4] J.N. Israelachvili, Intermolecular and Surface Forces, second ed., Academic Press, San Diego, 1992, chap. 17.

[5] K.A. Wilk, L. Syper, B. Burczyk, A. Sokołowski, B.W. Domagalska, J. Surfact. Deterg. 3 (2000) 185.

[6] B. Burczyk, K.A. Wilk, A. Sokołowski, L. Syper, J. Colloid Interface Sci. 240 (2001) 552.

[7] J. Eastoe, P. Rogueda, B.J. Harrison, A.M. Howe, A.R. Pitt, Langmuir 10 (1994) 4429.

[8] J. Eastoe, P. Rogueda, A.M. Howe, A.R. Pitt, R.K. Heenan, Langmuir 12 (1996) 2701.

[9] H. Andree, B. Middelhauve, Tenside Surfact. Deterg. 28 (1991) 413.

[10] P. Busch, H. Hensen, H. Tesmann, Tenside Surfact. Deterg. 30 (1993) 116.

[11] J.M. Pestman, K.R. Terpstra, M.C.A. Stuart, H.A. van Doren, A. Brisson, R.M. Kellogg, J.B.F.N. Engberts, Langmuir 13 (1997) 6857.

[12] M. Bergsma, M.L. Fielden, J.B.F.N. Engberts, J. Colloid Interface Sci. 243 (2001) 491.

[13] K.A. Wilk, L. Syper, B.W. Domagalska, U. Komorek, I. Maliszewska, R. Gancarz, J. Surfact. Deterg. 5 (2002) 235.

[14] U. Komorek, K.A. Wilk, J. Colloid Interface Sci. 271 (2004) 206.

[15] M.J.L. Castro, J. Kovensky, A.F. Cirelli, Langmuir 18 (2002) 2477.

[16] M.J.L. Castro, A.F. Cirelli, J. Kovensky, J. Surfact. Deterg. 9 (2006) 279.

[17] U. Laska, K.A. Wilk, I. Maliszewska, L. Syper, J. Surfact. Deterg. 9 (2006) 115.

[18] M. Johnsson, A. Wagenaar, J.B.F.N. Engberts, J. Am. Chem. Soc. 125 (2003) 757.

[19] M. Johnsson, A. Wagenaar, M.C.A. Stuart, J.B.F.N. Engberts, Langmuir 19 (2003) 4609.

[20] M. Scarzello, J.E. Klijn, A. Wagenaar, M.C.A. Stuart, R. Hulst, J.B.F.N. Engberts, Langmuir 22 (2006) 2558.

[21] K.A. Wilk, L. Syper, B. Burczyk, I. Maliszewska, M. Jon, B. Domagalska, J. Surfact. Deterg. 4 (2001) 155.

[22] F.M. Menger, B.N.A. Mbadugha, J. Am. Chem. Soc. 123 (2001) 875.

[23] K. Nyuta, T. Yoshimura, K. Tsuchiya, T. Ohkubo, H. Sakai, M. Abe, K. Esumi, Langmuir 22 (2006) 9187.

[24] T. Yoshimura, K. Ishihara, K. Esumi, Langmuir 21 (2005) 10409.

[25] K. Kalyansundaram, J.K. Thomas, J. Am. Chem. Soc. 99 (1977) 2039.

[26] K.P. Ananthapadmanabhan, E.D. Goddard, N.J. Turro, P.L. Kuo, Langmuir 1 (1985) 352.

[27] M. Borkovec, in: K. Holmberg (Ed.), Handbook of Applied Surface and Colloid Chemistry, Wiley, New York, 2001, chap. 18.

[28] E. Alami, G. Beinert, P. Marie, R. Zana, Langmuir 9 (1993) 1465.

[29] E. Alami, K. Holmberg, J. Eastoe, J. Colloid Interface Sci. 247 (2002) 447.

[30] M.J. Rosen, Surfactants and Interfacial Phenomena, third ed., Wiley, New York, 2004.

[31] A.F. Ward, L. Tordai, J. Phys. Chem. 14 (1946) 453.

[32] R.S. Hansen, J. Phys. Chem. 64 (1960) 637.

[33] E. Rillaerts, P. Joos, J. Phys. Chem. 86 (1982) 3471.

[34] V.B. Fainerman, A.V. Makievski, R. Miller, Colloids Surf. A 87 (1994) 61.

[35] J. Eastoe, J.S. Dalton, Adv. Colloid Interface Sci. 85 (2000) 103.

[36] T. Yoshimura, K. Nyuta, K. Esumi, Langmuir 21 (2005) 2682.

[37] A. Bernheim-Groswasser, R. Zana, Y. Talmon, J. Phys. Chem. B 104 (2000) 4005.

Available online at www.sciencedirect.com
ScienceDirect
Journal of Colloid and Interface Science 312 (2007) 139–145
JOURNAL OF Colloid and Interface Science
www.elsevier.com/locate/jcis

Phase behavior of mixed solution of a glycerin-modified cationic surfactant and an anionic surfactant

Koji Tsuchiya [a], Jun Ishikake [a], Tae Seong Kim [b], Takahiro Ohkubo [c], Hideki Sakai [a,c], Masahiko Abe [a,c,*]

[a] *Faculty of Science and Technology, Tokyo University of Science, 2641 Yamazaki, Noda, Chiba 278-8510, Japan*
[b] *Cognis Korea Ltd., Kangnam Metro Bldg. 1339-9, Seocho-Ku, Seoul 137-860, Republic of Korea*
[c] *Institute of Colloid and Interface Science, Tokyo University of Science, 1-3 Kagurazaka, Shinjuku, Tokyo 162-8601, Japan*

Received 2 June 2006; accepted 28 July 2006
Available online 2 August 2006

Abstract

The phase behavior of mixed solution of newly synthesized monoglycerylcetyldimethylammonium chloride (MGCA) and sodium octyl sulfate (SOS) in water was investigated by cryo-transmission electron microscopy (cryo-TEM), dynamic light scattering (DLS), differential scanning calorimetry (DSC), and fluorescence polarizing for evaluation of the microviscosity of bilayers. No precipitate was observed in the mixed solution except at concentrations below 20 mM over all mixing ratios, and stable vesicles were formed in a considerably wide range of mixing ratio, even at the equimolar ratio. Vesicles formed in aqueous 1/1 MGCA/SOS mixture were found to exhibit no phase transition, and fluorescence polarizing measurements showed that the vesicle bilayers have a high fluidity. This flexibility allows the bilayers to have a spontaneous curvature, and thus vesicles rather than flat lamellae can be stabilized in the mixture even at the equimolar ratio. In addition, because the glycerin group of MGCA interacts strongly with water, the hydration repulsion contributes to prevent the bilayers consisting of MGCA and SOS from adhering and flocculating even though the charge neutralization between MGCA and SOS occurs at the equimolar ratio.
© 2006 Elsevier Inc. All rights reserved.

Keywords: Catanionic surfactant; Glycerin-modified surfactant; Thermodynamically stable vesicles

1. Introduction

Aqueous mixtures of anionic and cationic surfactants exhibit many peculiar properties that are not possessed by the other combinations of mixed surfactants. Strong synergistic interactions occur in dilute solutions of mixed cationic and anionic surfactants. The mixed system thus exhibits a drastic decrease in the critical aggregation concentration (cac) value at different mixing rations relative to the critical micelle concentration (cmc) of either of pure components. In addition, the mixture has a lowest attainable surface tension (γ_{cmc}) lower than those of single components [1–6]. The high interfacial activity of the system can be useful for its industrial applications as new detergents, emulsifiers, and dispersants.

Moreover, mixtures of oppositely charged surfactants self-assemble into a variety of aggregates [7–19] such as spherical micelles, rod-like micelles, disks, vesicles, and lamellar liquid crystals depending on the strength of intermolecular interactions, the geometrical shape of surfactant species, the mole fraction of oppositely charged surfactants, and concentration. Of particular interest for these mixtures is spontaneous formation of vesicles in dilute solutions. Since Kaler and co-workers [7] first reported such spontaneous formation of thermodynamically stable vesicles in anionic and cationic mixed surfactant systems, many researchers have investigated the microstructures and properties of spontaneously formed vesicles because they are expected to be used as a drug delivery system, model membrane, microreactor for production of colloidal assemblies, and cosmetics. When solutions of anionic and cationic surfactants are simply mixed, ion pairing of both surfactants induces vesicle formation at appropriate molar ratios even at low concentrations [7,8]. Because charge neutralization due to the ion

* Corresponding author. Fax: +81 4 7124 8650.
E-mail address: abemasa@rs.noda.tus.ac.jp (M. Abe).

0021-9797/$ – see front matter © 2006 Elsevier Inc. All rights reserved.
doi:10.1016/j.jcis.2006.07.075

pairing causes a smaller area per head group for the mixed surfactants than the sum of those areas for the single surfactants, the critical packing parameter (CPP) [20,21] for the mixture is large compared with that for the individual surfactants, and the catanionic ion pair can thus be a favorable geometrical structure to form bimolecular membranes [7,8].

Yet, aqueous mixtures of anionic and cationic surfactants have a serious drawback for their practical use that insoluble catanionic surfactant salts formed in the solution are generally precipitated at around the equimolar mixing ratio, even though they have excellent solution properties such as high interfacial activity and spontaneous vesicle forming ability. We have so far reported the effect of temperature on the phase behavior of aqueous mixtures of cetyltrimethylammonium bromide (CTAB) and sodium octyl sulfate (SOS) [22]. For this mixed surfactant system, an increase in temperature above the gel (L_β)–liquid crystalline (L_α) transition temperature of the CTA^+/OS^- complex permits a shrink in the precipitation region and an appreciable enhancement in the vesicle region [22].

In the present study, we synthesize a cationic alkyl quaternary ammonium salt modified with glycerin at the head group, in order to prevent precipitate formation when the cationic surfactant is mixed with anionic surfactant. We also report here the phase behavior of aqueous mixture of newly synthesized monoglycerylcetyldimethylammonium chloride (MGCA) and sodium octyl sulfate (SOS).

2. Materials and methods

2.1. Materials and preparation

Monoglycerylcetyldimethylammonium chloride (MGCA, Scheme 1) was synthesized in the following way. *N*,*N*-dimethylcetylamine (Tokyo Chemical Industry, Co., Ltd.) was allowed to react with 3-chloro-1,2-propanediol (Tokyo Chemical Industry, Co., Ltd.) in 2-propanol (Wako Pure Chemical Industries, Ltd.) at 90–100 °C for 6 h. The solvent was removed by evaporation, and *n*-butanol (Wako Pure Chemical Industries, Ltd.) was added to the residue. The solution obtained was poured into water saturated with sodium chloride (Wako Pure Chemical Industries, Ltd.) in a separating funnel, which was then shaken vigorously. The lower aqueous phase was separated, and *n*-butanol in the upper organic phase was removed by distillation. No glycerin was detected in the upper phase by TLC. The residue obtained after distillation was recrystallized 3 times from acetone–ethanol mixture to give white powder with a high purity. ^{1}H NMR ($CDCl_3$, 300 MHz): $\delta = 0.86$ (3H, t, CH_3–$(CH_2)_{14}$–), 1.25 (28H, m, –$(CH_2)_{14}$–), 1.78 (2H, d, –$(CH_2)_{14}$–CH_2–N^+), 3.33 (6H, t, –$N^+(CH_3)_2$–CH_2–), 3.44–3.82 (4H, m, –CH_2–CH(OH)–CH_2–), 4.42 (1H, b, –CH_2–CH(OH)–CH_2–), 4.83 (1H, d, –CH_2–CH(OH)–CH_2–), 5.78 (1H, t, –CH_2–OH); Fab + m/z 288.0000.

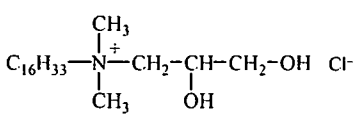

Scheme 1. Monoglycerylcetyldimethylammonium chloride (MGCA).

Cetyltrimethylammonium chloride (CTAC, Tokyo Chemical Industry Co., Ltd.) was used as the reference cationic surfactant for MGCA after being purified by recrystallization from 1:1 mixture of acetone and ethanol. Sodium octyl sulfate (SOS, Sigma–Aldrich Chemical Co.) was used as supplied as the anionic surfactant. All preparations were conducted using Milli-Q water. First, samples were prepared by making stock solutions of both cationic and anionic surfactants at the desired concentration and then mixing them in the desired molar ratios under stirring with a vortex mixer for 5 s. No strong external force such as ultrasonic irradiation was applied in the preparation. The mixed solutions thus prepared were allowed to stand at 20 °C.

2.2. Surface tension measurement

Equilibrium surface tensions of surfactant solutions were measured with a Wilhelmy surface tensiometer (Model CBVP-Z, Kyowa Interface Science Co., Ltd.) using a platinum plate at 25 °C.

2.3. Cryogenic transmission electron microscopy (cryo-TEM) [23,24]

A small amount (3–5 μl) of sample solution for cryo-TEM was placed on the surface of a TEM copper grid covered by a holey carbon film, which was held by a pair of self-locking tweezers mounted on a spring-loaded shaft with a cryo-preparation system (LEICA EM CPC, LEICA microsystems). An excess amount of sample drop was blotted away by touching it with a filter paper to form a thin liquid film on the grid (<300 nm). The thin liquid film on the grid was immediately vitrified by plunging it into liquid ethane (−175 °C) cooled with liquid nitrogen. Then, the grid was transferred onto the tip of a cryospecimen holder (CT-3500, Oxford Instruments) in liquid nitrogen. Specimens were kept at about −173 °C and imaged in a transmission electron microscope (H-7650, Hitachi Science Systems, Ltd.) at an accelerating voltage of 120 kV under low electron dose.

2.4. Dynamic light scattering (DLS) measurement

Sample solutions for DLS measurements were prepared by mixing the stock solutions of cationic and anionic surfactants after passing them through a polycarbonate filter with a pore size of 0.2 μm. Hydrodynamic diameter and particle size distribution were measured with a dynamic light scattering measuring apparatus (NICOMP 380 ZLS, Particle Sizing Systems) at a scattering angle 90° using a wavelength 535 nm.

2.5. Differential scanning calorimetry (DSC)

DSC measurements were performed with a differential scanning calorimeter (DSC 8230, Rigaku Co.) at a heating rate of 1 K/min. A stainless steel pan was used as the sample vessel.

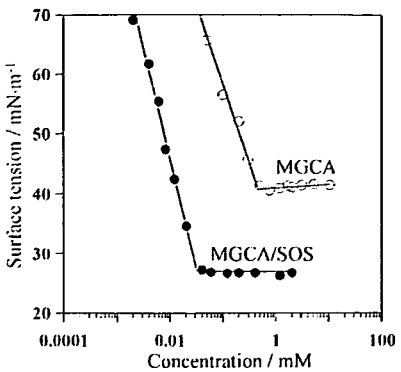

Fig. 1. Surface tension curves for aqueous solutions of pure MGCA and mixed MGCA/SOS at 25 °C.

The reference was Milli-Q water with the same weight as that of the sample.

2.6. Fluorescence polarization measurement

The microviscosity of bimolecular membranes was determined through fluorescence polarization measurements using 1,6-diphenyl-1,3,5-hexatrience (DPH) as a fluorescence probe. DPH dissolved in tetrahydrofuran was added to samples to make DPH/surfactants molar ratio 1/500. The solutions containing DPH were incubated at 37 °C for 1 h to solubilize the probe in the bimolecular membranes of aggregates, and then the fluorescence intensity was measured with a fluorescence spectrophotometer (RF-5000, Shimadzu Co.). The excitation and emission wavelengths were 350 and 450 nm, respectively. Fluorescence polarization (P) was calculated using the following equation:

$$P = (I_p - GI_v)/(I_p + GI_v),$$

where I_p and I_v are the fluorescence intensities of emitted light polarized parallel and vertical to exciting light, respectively, and G is the grating correction factor [25]. DPH is solubilized in the hydrophobic region of the bimolecular membrane and thus allows us to evaluate the microviscosity around DPH. Fluorescence polarization is correlated to the microviscosity near the fluorescent probe [26–28], which is calculated using Perrin–Weber's equation [29,30]. An increase in fluorescence polarization corresponds to an increase in the microviscosity of the hydrophobic part of membrane.

3. Results and discussion

3.1. Surface tension of aqueous MGCA/SOS solution

Fig. 1 shows surface tension versus the logarithm of concentration plots for pure MGCA solution and mixed MGCA/SOS aqueous solution at the equimolar ratio. The critical micelle concentration (cmc) and critical aggregation concentration (cac) for aqueous pure MGCA and MGCA/SOS solutions were determined from the break in these plots. The cmc of pure MGCA was 0.5 mM and the value of surface tension at the cmc (γ_{cmc}) was 41 mN/m. There was no minimum in the surface

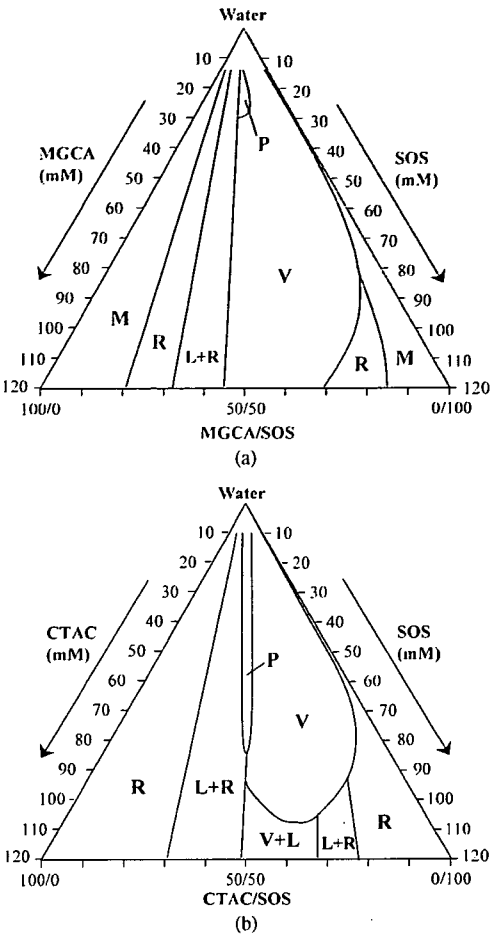

Fig. 2. Ternary phase diagrams for (a) MGCA/SOS/H_2O and (b) CTAC/SOS/H_2O at 20 °C. (M, spherical micelles; R, rod-like micelles; V, vesicles; L, lamellar liquid crystals; and P, precipitate.) All samples were prepared on the molar concentration basis and equilibrated at 20 °C for more than 3 months.

tension versus concentration curve for pure MGCA solution, a fact suggesting that the surfactant solution does not contain surface active impurities. The cmc and γ_{cmc} of pure SOS were reported to be 120 mM and 40 mN/m in the previous report [9], respectively. The cac for equimolar mixture of MGCA and SOS was 0.03 mM, which is one order of magnitude lower than that of pure MGCA and four orders of magnitude lower than that of pure SOS. In addition, the equimolar mixture showed a γ_{cmc} value (27 mN/m) lower than either of pure MGCA and SOS solution. This strong anionic–cationic synergism is likely to be caused by the adsorption of 1/1 $MGCA^+/OS^-$ catanionic surfactant at the air/water interface, which is more hydrophobic than either of two pure ionic components [1,6,9].

3.2. Phase behavior of aqueous mixture of MGCA and SOS

Fig. 2a shows the ternary phase diagram of a dilute solution of mixed MGCA and SOS. All samples were left standing for more than 3 months after preparation in a thermostated bath at 20 °C to attain an equilibrium state [9]. The phase behavior was examined by visual, differential interference optical microscopic, cross polarized light microscopic, and cryo-TEM

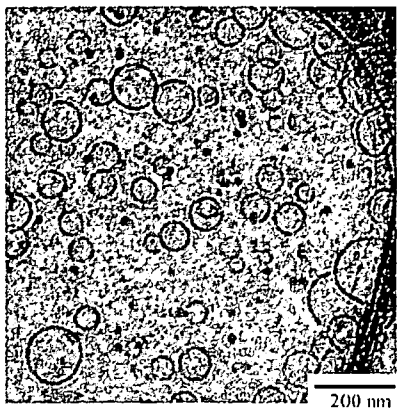

Fig. 3. Cryo-TEM micrograph of aqueous MGCA/SOS mixture with equimolar mixing ratio (total surfactant concentration of 50 mM).

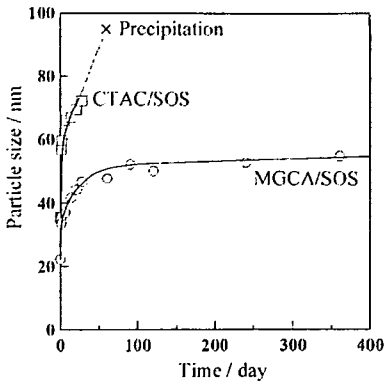

Fig. 4. Changes in mean hydrodynamic diameter of aggregates with time for aqueous mixtures of MGCA/SOS and CTAC/SOS at molar ratio of 1/1 and total surfactant concentration of 50 mM measured with dynamic light scattering (DLS).

observations. When SOS was added to pure MGCA micellar solution, mixed spherical micelles (M) were formed in the solution. With further addition of SOS, viscous solutions were obtained, a fact suggesting the formation of rod-like micelles (R) [9]. When the SOS molar ratio, X_{SOS}, was increased beyond those in the R region, samples separated into two phases. The upper phase was turbid and consisted of cloud-like wisps [8,9], while the lower one was viscous. The cloud-like wisps formed in the upper layer are likely to be lamellar liquid crystals (L) because Maltese cross patterns were observed by cross polarized light microscopy.

A characteristic and interesting phase behavior was obtained on the SOS-rich side. When a small amount of MGCA was mixed with pure SOS monomeric solution (<50 mM), vesicles were formed in the dilute mixed solution as described for aqueous solution of a decyltrimethylammonium bromide (DeTAB) and sodium decyl sulfate (SDeS) mixture by Villeneuve and co-workers [6]. At total surfactant concentrations lower than 50 mM, a one-phase region of vesicle (V) was found at almost all SOS-rich compositions. These mixed solutions were bluish and slightly turbid, and the appearance remained unchanged for many months. In particular, no precipitate was observed even at the equimolar ratio in the mixed solution except at concentrations below 20 mM. The aggregation state of aqueous mixture of MGCA/SOS prepared at the equimolar ratio was investigated by cryo-TEM. Small unilamellar vesicles (SUVs) were observed on the cryo-TEM micrograph (Fig. 3). These vesicles had diameters ranging from 30 to 100 nm. Small dot-like objects (~30 nm) on the micrograph are likely to be small ice-crystals because the size distribution by DLS revealed that no aggregates with smaller size (⩽30 nm) are formed in the solution. Vesicles formed in the SOS-rich corner were transformed into spherical micelles (M) or rod-like micelles (R) at high surfactant concentrations.

Fig. 2b shows the ternary phase diagram of an aqueous mixture of CTAC, a typical cationic surfactant, and SOS at 20 °C. The phase behavior of aqueous CTAC/SOS mixtures was compared with that of aqueous MGCA/SOS mixture. A large difference in phase behavior was found between aqueous CTAC/SOS and MGCA/SOS mixtures. Crystalline precipitates (P) were found for the aqueous mixture of CTAC and SOS (<80 mM) around the equimolar mixing ratio as observed with many anionic and cationic mixed surfactant systems. The vesicle forming region (V) for CTAC/SOS/H_2O system was narrow compared with that for MGCA/SOS/H_2O system.

The above findings demonstrate an appreciate effect of the glycerin group of MGCA on the phase behavior of aqueous mixture of anionic and cationic surfactants. Vesicles formed in aqueous MGCA/SOS mixtures are stabilized even at the equimolar ratio, and the vesicle region covers a considerably wide range. Then we investigate the difference in solution properties between aqueous MGCA/SOS and CTAC/SOS mixtures at the equimolar ratio.

3.3. Dynamic light scattering (DLS) measurement

DLS measurements were performed to investigate the dispersion stability of aggregates of MGCA/SOS/H_2O and CTAC/SOS/H_2O systems prepared at the equimolar ratio. Fig. 4 shows the mean hydrodynamic diameters of the aggregates as a function of time after their preparation. Initially, the equimolar mixture of CTAC/SOS had a mean hydrodynamic aggregate diameter of 35 nm. The mean diameter rapidly increased in several hours after preparation, and finally precipitates appeared in the solution after 1 month. In contrast, for the equimolar MGCA/SOS solution, the mean diameter increased from 20 to 50 nm in the first 3 months and thereafter remained unchanged for at least 9 months. The mean diameter measured by DLS after attaining equilibrium was almost consistent with the average diameter of SUVs observed by cryo-TEM. DLS data described above indicate that vesicles consisting of MGCA and SOS at the 1/1 molar ratio are dispersed stably in water.

3.4. Differential scanning calorimetry (DSC) and fluorescence polarization measurement

The difference in membrane property between MGCA/SOS/H_2O and CTAC/SOS/H_2O systems prepared at the equimolar ratio was investigated by DSC and fluorescence polarizing

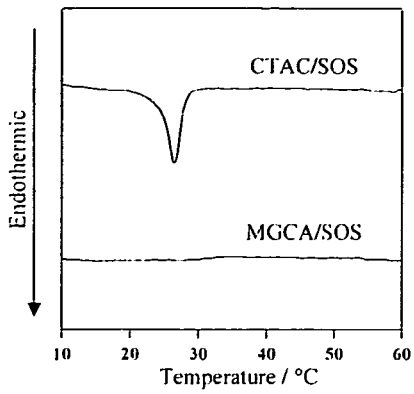

Fig. 5. DSC heating curves of aqueous mixtures of MGCA/SOS and CTAC/SOS at molar ratio of 1/1 (total surfactant concentration of 50 mM).

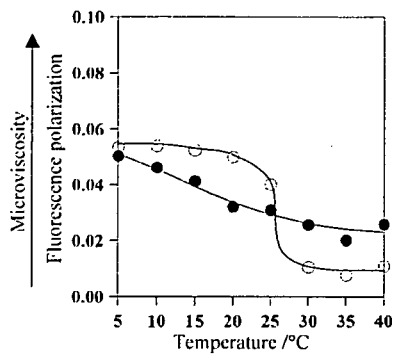

Fig. 6. Temperature dependence of fluorescence polarization for MGCA/SOS and CTAC/SOS aqueous mixtures at equimolar ratio and total surfactant concentration of 50 mM. Fluorescence probe, 1,6-diphenyl-1,3,5-hexatriene (DPH), is located in the hydrophobic region of bimolecular membranes, and its fluorescence polarization enables us to evaluate the microviscosity around the probe.

using DPH as a fluorescence probe. Fig. 5 shows the DSC heating curves for aqueous MGCA/SOS and CTAC/SOS mixtures at the equimolar ratio. An endothermic peak was observed at 24.8 °C for aqueous 1/1 CTAC/SOS solution. This phase transition corresponds to the gel (L_β)-liquid crystal (L_α) phase transition of CTAC/SOS bilayer membranes, as we reported for aqueous mixture of cetyltrimethylammonium bromide (CTAB) and sodium octyl sulfate (SOS) [22]. On the other hand, aqueous MGCA/SOS mixture had no endothermic peak in the temperature range measured (10–60 °C).

Fig. 6 shows the temperature dependence of fluorescence polarization of DPH. Fluorescence polarization of DPH incorporated into bilayer membranes is related to the microviscosity of the bilayer. The fluorescence polarization of DPH in CTAC/SOS equimolar mixture suddenly decreased above 25 °C, in good agreement with the phase transition temperature obtained by DSC. This sudden reduction in fluorescence polarization indicates that the packing of CTAC/SOS bilayers becomes loose, a fact strongly suggesting the phase transition from L_β phase to L_α phase of the bimolecular membranes. In contrast, fluorescence polarization gradually decreased with increasing temperature for equimolar mixture of MGCA/SOS. This finding suggests that no defined phase transition occurs in MGCA/SOS mixed surfactant system. In addition, the microviscosity of MGCA/SOS bilayers was low compared with that of CTAC/SOS bilayers at 20 °C.

3.5. Vesicle stabilization in aqueous 1/1 MGCA/SOS mixture

There is a large difference in phase behavior between MGCA/SOS/H_2O and CTAC/SOS/H_2O systems, especially at the equimolar ratio. The introduction of glycerin to the head group of cationic quaternary ammonium-type surfactants leads to vesicle stabilization of the catanionic surfactants even at the equimolar ratio. Several factors have been reported to affect the formation of stable vesicles. Critical packing parameter (CPP) [20,21] is useful for us to predict what kind of aggregates are favorably formed by surfactant molecules.

$$\mathrm{CPP} = V/a_0 l_c,$$

where V is the volume of the hydrophobic portion, a_0 is the effective area per hydrophilic group, and l_c is the length of the hydrophobic group. CPP value is related to the allowable aggregate geometry for surfactant molecules as given below: spherical micelle, CPP < 1/3; cylindrical micelle, 1/3 < CPP < 1/2; vesicle 1/2 < CPP < 1; planer bilayer, CPP ~ 1; inverted micelle, CPP > 1 [20,21].

For anionic and cationic mixed surfactant systems, pseudo-double-tailed ion pairs of oppositely charged surfactants, which have a geometrical structure (CPP) favorable to bilayer, are formed by the electrostatic attraction between the head groups [7,8]. Because MGCA has a larger head group than CTAC, the CPP value of $MGCA^+/OS^-$ ion pair is expected to be smaller than that of CTA^+/OS^- ion pair. Thus, $MGCA^+/OS^-$ ion pairs are likely to have a possible geometry to form vesicles (1/2 < CPP < 1), while CTA^+/OS^- ion pairs are favorable to form planer bilayers (CPP ~ 1). This is one of the possible reasons why MGCA/SOS vesicles are stabilized in the solution at the equimolar ratio. Yet, we cannot fully explain the vesicle stabilization only by the CPP theory.

The curvature energy of bimolecular membrane is related to the formation of thermodynamically stable vesicles. Several researchers [8,31–34] reported an important contribution of the bending energy of a vesicle bilayer to determine whether spontaneous vesicles or planar lamellar phases are formed in water. In the case of planar lamella, the hydrocarbon chains of surfactants located at the edge of the membrane have a cost in free energy because they are exposed to water. Although this edge energy is excluded by the deformation of the membrane into a closed shape (vesicle), the bilayer curvature requires bending energy.

Safran and co-workers [32,33] reported the curvature energy required to bend a flat bilayer with the viewpoint of the spontaneous curvature of the inner and outer monolayers constituting the bilayer. The curvature elastic energy of the vesicle per unit area (E) is given by

$$E = 2K\left[(c + c_0)^2 + (c - c_i)^2\right],$$

where K is curvature elastic modulus, and c, c_i, and c_0 are the spontaneous curvatures of vesicle bilayer, inner, and outer

monolayers constituting the bilayer, respectively. In the case of bilayers consisting of a single surfactant, planer lamellar phases are usually preferable to vesicles because the inner and outer monolayers have opposite spontaneous curvatures regarding signs [32,33]. However, when two oppositely charged surfactants are mixed in water, nonideal mixing of these surfactants in the inner and outer monolayers permits the spontaneous formation of vesicles [31], that is, excess surfactant molecules, which do not form a catanionic surfactant complex with the other component, preferentially orient in the outer monolayer.

In the present study, mixing MGCA with SOS leads to the formation of vesicles even at the equimolar mixing ratio at 20 °C. At this mixing ratio, the nonideal mixing of these two components does not relate to vesicle stabilization, and then the bending elastic modulus is likely to an important factor. As shown in DSC and fluorescence polarization measurements, the microviscosity of the vesicle bilayer for aqueous 1:1 MGCA/SOS solution is considerably low at 20 °C. Such soft and flexible membranes with low K can be rounded into a vesicle due to entropy stabilization [34,35]. On the other hand, bimolecular membranes consisting of CTAC and SOS at the equimolar ratio are gel phase (L_β) with a low membrane fluidity at 20 °C, thereby resulting in the formation of planar lamellar phases as precipitate rather than vesicles with a closed shape. The microviscosity decreased significantly at the gel–liquid crystal transition temperature (T_c: 24.8 °C), and is lower than that for MGCA/SOS mixture at temperatures above T_c. However, precipitate was observed in the equimolar mixture even at higher temperatures [22]. Poor dispersion stability induced by the charge neutralization described as the following is likely to cause the formation of planar lamellae relative to vesicles.

Next, we consider the effect of the interactions between two bilayers on vesicle stabilization. Many researchers have reported a lot of repulsive interactions which prevent bilayer membranes from adhering and flocculating, such as electrostatic repulsions [20,36–38], hydration interactions [20,39–43], undulation interactions [20,34,42–46], and protrusion interactions [20,47–49].

The bilayer–bilayer repulsion for equimolar CTAC/SOS mixture is so small that vesicles flocculate and grow to be planar lamella because the electric charge is neutralized.

In contrast, DLS data for aqueous MGCA/SOS solution at the equimolar ratio showed that vesicles formed in the mixture are stable for a long time over 3 months after preparation. The hydration repulsion between the bilayers largely contributes to vesicle stabilization because the glycerin group of MGCA interacts strongly with water even though the charge neutralization between MGCA and SOS occurs at the equimolar ratio. In addition, soft and flexible vesicle membranes consisting of MGCA and SOS easily undulate by themselves. Helfrich and co-workers reported that the undulation force between two membranes per unit area is reversely proportional to curvature elastic modulus [34,46]. Thus the undulation repulsion also seems to be related to the formation of stable vesicles consisting of catanionic MGCA/SOS surfactants.

4. Summary

Vesicles are stabilized for a long time in aqueous mixtures of MGCA and SOS even though the electric charges of these surfactants are neutralized at the equimolar ratio, and the vesicle region covers a considerably wide range. The glycerin group of MGCA induces the formation of flexible bimolecular membranes for catanionic surfactant solutions, which suggests that the bilayers can easily be rounded into vesicles. In addition, an enhancement in the repulsive interactions between bilayers such as the hydration force on the glycerin group of MGCA and the undulation force based on the membrane flexibility is responsive for the vesicle stabilization in aqueous MGCA/SOS mixtures. The findings obtained in the present study would be helpful for practical applications of anionic and cationic mixed surfactant systems which have a high dispersion stability and excellent interfacial activity as new detergents, cosmetics and emulsifiers.

References

[1] E.H. Laucassen-Reynders, J. Lucassen, D. Giles, J. Colloid Interface Sci. 81 (1981) 150.
[2] X.-G. Li, F.-M. Liu, Colloids Surf. A 96 (1995) 113.
[3] L.-H. Zhang, G.-X. Zhao, J. Colloid Interface Sci. 127 (1989) 353.
[4] A. Khan, C. Mendonca, J. Colloid Interface Sci. 169 (1995) 60.
[5] S. Backlund, R. Friman, S. Karlsson, Colloids Surf. A 123 (1997) 125.
[6] M. Villeneuve, S. Kaneshina, T. Imae, M. Aratono, Langmuir 15 (1999) 2029.
[7] E.W. Kaler, A.K. Murthy, B.E. Rodriguez, J.A.N. Zasadzinski, Science 245 (1989) 1371.
[8] E.W. Kaler, K.L. Herrington, A.K. Murthy, J.A.N. Zasadzinski, J. Phys. Chem. 96 (1992) 6698.
[9] M.T. Yatcilla, K.L. Herrington, L.L. Brasher, E.W. Kaler, S. Chiruvolu, J.A.N. Zasadzinski, J. Phys. Chem. 100 (1996) 5874.
[10] D.J. Iampietro, L.L. Brasher, E.W. Kaler, A. Stradner, O. Glatter, J. Phys. Chem. B 102 (1998) 3105.
[11] R.D. Koehler, S.R. Raghavan, E.W. Kaler, J. Phys. Chem. B 104 (2000) 11035.
[12] Y. Xia, I. Goldmints, P.W. Johnson, T.A. Hatton, A. Bose, Langmuir 18 (2002) 3822.
[13] E. Marques, A. Khan, M.G. da Miguel, B. Lindman, J. Phys. Chem. 97 (1993) 4729.
[14] Y. Kondo, H. Uchiyama, N. Yoshino, K. Nishiyama, M. Abe, Langmuir 11 (1995) 2380.
[15] K. Tsuchiya, H. Sakai, T. Saji, M. Abe, Langmuir 19 (2003) 9343.
[16] M. Bergström, J.S. Pedersen, P. Schurtenberger, S.U. Egelhaaf, J. Phys. Chem. B 103 (1999) 9888.
[17] J. Hao, Z. Yuan, W. Liu, H. Hoffmann, J. Phys. Chem. B 108 (2004) 5105.
[18] K. Horbaschek, H. Hoffmann, C. Thunig, J. Colloid Interface Sci. 206 (1998) 439.
[19] T. Zemb, M. Dubois, B. Demé, T. Gulik-Krzywicki, Science 283 (1999) 816.
[20] J.N. Israelachvili, Intermolecular and Surface Forces, second ed., Academic Press, San Diego, 1992.
[21] J.N. Israelachvili, D.J. Mitchell, B.W. Ninham, J. Chem. Soc. Faraday Trans. II 72 (1976) 1525.
[22] K. Tsuchiya, H. Nakanishi, H. Sakai, M. Abe, Langmuir 20 (2004) 2117.
[23] J.R. Bellare, H.T. Davis, L.E. Scriven, Y. Talmon, J. Electron Microsc. Technol. 10 (1988) 87.
[24] M. Almgren, K. Edwards, G. Karlsson, Colloids Surf. A 174 (2000) 3.
[25] T. Inoue, Y. Muraoka, K. Fukushima, R. Shimozawa, Chem. Phys. Lipids 46 (1988) 107.

[26] K. Kinoshita, R. Kataoka, Y. Kimura, O. Gotoh, A. Ikegami, Biochemistry 20 (1981) 4270.
[27] E.L. Pugh, R. Bittman, L. Fugler, M. Kates, Chem. Phys. Lipids 50 (1989) 43.
[28] M. Abe, M. Goto, K. Ogino, J. Jpn. Oil Chem. Soc. 39 (1990) 351.
[29] P. Wahl, G. Weber, J. Mol. Biol. 30 (1967) 371.
[30] J.K. Weltman, G.M. Edelman, Biochemistry 6 (1967) 1437.
[31] W.Z. Helfrich, Naturforsch C 28 (1973) 693.
[32] S.A. Safran, P.A. Pincus, D. Andelman, Science 284 (1990) 354.
[33] S.A. Safran, P.A. Pincus, D. Andelman, D.C. MacKintosh, Phys. Rev. A 43 (1991) 1071.
[34] W.Z. Helfrich, Naturforsch A 33 (1978) 305.
[35] D.D. Lasic, Nature 355 (1992) 279.
[36] R.M. Pashley, J.N. Israelachvili, Colloids Surf. 2 (1981) 169.
[37] R.M. Pashley, B.W. Ninham, J. Phys. Chem. 91 (1987) 2902.
[38] J. Marra, J. Colloid Interface Sci. 107 (1985) 446.
[39] D.M. LeNeveu, R.P. Rand, V.A. Parsegian, D. Gingell, Nature 259 (1976) 601.
[40] T.J. McIntosh, S.A. Simon, Biochemistry 25 (1986) 4058.
[41] J.N. Israelachvili, R.M. Pashley, Nature 300 (1982) 341.
[42] R.M. Pashley, P.M. McGuiggan, B.W. Ninham, D.F. Evans, Science 229 (1985) 1088.
[43] J. Marra, J.N. Israelachvili, Biochemistry 24 (1985) 4608.
[44] W. Helfrich, J. Phys. 46 (1985) 1263.
[45] J.O. Rädler, T.J. Feder, H.H. Strey, E. Sackmann, Phys. Rev. E 51 (1995) 4526.
[46] R.M. Servuss, W. Helfrich, J. Phys. France 50 (1989) 809.
[47] E.A.G. Aniansson, S.N. Wall, M. Almgren, H. Hoffmann, I. Kielmann, W. Ulbricht, R. Zana, J. Lang, C. Tondre, J. Phys. Chem. 80 (1976) 905.
[48] E.A.G. Aniansson, J. Phys. Chem. 82 (1978) 2805.
[49] J.N. Israelachvili, H. Wennerström, Langmuir 6 (1990) 873.

Apoptosis
DOI 10.1007/s10495-007-0053-0

Conformational change in the active center region of GST P1-1, due to binding of a synthetic conjugate of DXR with GSH, enhanced JNK-mediated apoptosis

Tadashi Asakura · Atsuko Sasagawa · Hitoshi Takeuchi · Shun-ichi Shibata · Hideki Marushima · Satoshi Mamori · Kiyoshi Ohkawa

© Springer Science + Business Media, LLC 2007

Abstract Treatment of cells with a synthetic conjugate of DXR with GSH via glutaraldehyde (GSH-DXR) caused cytochrome *c* to be released from the mitochondria to the cytosol following potent activation of caspase-3 and -9 by typical DNA fragmentation. This apoptosis was regulated by the JNK-signaling pathway. In the present experiment, binding of GSH-DXR to GST P1-1 allosterically led to the disappearance of its enzyme activity and activated the kinase activity of JNK without dissociation of the JNK-GST P1-1 complex. The recombinant GST P1-1 molecule with a mutation in the active center region (W38H and C47S) lost its GST activity when bound to JNK to the same degree as the wild-type, with the mutated GST P1-1 molecule failing to inhibit the activity of JNK. It has been reported that JNK-signaling is regulated by GST P1-1 via interaction with the C-terminus. We confirmed that GST P1-1 deletion mutant (Δ194–209) and a site-directed mutant (R201A) in the C-terminal region failed to bind and inhibit JNK. These results indicated that not only binding of the C-terminal region of GST P1-1 to the JNK molecule, but also the active center region of GST P1-1 play important roles in the regulation of JNK enzyme activity. The findings suggested that allosteric inhibition of GST P1-1 activity by the binding of GSH-DXR following conformational change may activate JNK and induce apoptosis via the mitochondrial pathway in the cells.

Keywords Apoptosis · c-Jun N-terminal kinase · Doxorubicin · Glutathione-Doxorubicin conjugate · Glutathione S-transferase P1-1 · Rat hepatoma cell

T. Asakura (✉) · A. Sasagawa · H. Takeuchi · S.-i. Shibata · H. Marushima · S. Mamori · K. Ohkawa
Department of Biochemistry (I),
Jikei University School of Medicine,
3-25-8 Nishi-shinbashi,
Minato-ku,
Tokyo 105-8461, Japan
e-mail: tad_asakura@jikei.ac.jp

A. Sasagawa · H. Takeuchi
Department of Pharmaceutical Therapeutics,
Kyoritsu College of Pharmacy, Tokyo 105-8512

Introduction

The stress-activated protein kinase, c-Jun N-terminal kinase (JNK), is predominantly activated by inflammatory cytokines and stress stimuli through phosphorylation of 183T and 185Y, and its active center consisting of an ATP-binding site formed by 55K [1–4]. The importance of the JNK pathway has also been shown in the control of cell survival and death pathways, and interference with the JNK pathway suppresses induction of apoptosis by a variety of agents [5]. Recently, the link between the redox active components of glutathione S-transferase P1-1 (GST P1-1, placental type isozyme of rat GST), and stress-activated kinases, such as JNK, has been redefined as a non-catalytic, ligand binding activity that mediates both stress and apoptotic responses [5–9]. It was important for the induction of cell proliferation, differentiation and apoptosis to activate JNK [10–14]. Strong and prolonged activation of JNK has been reported in response to lethal doses of a variety of stresses including UVC, γ radiation and cisplatin, any one of which triggers apoptosis [10–14]. It has been reported that JNK bound to several non-substrate proteins, including $p21^{WAF1}$, JIP, Rb, Hsp72 and GST P1-1 [6, 7, 15–17]. It has also been shown that $p21^{WAF1}$, Rb, Hsp72 and GST P1-1 inhibit JNK through protein-protein interactions [6, 7, 15–17], whereas JIP serves as a scaffolding protein in the JNK pathway [18]. It was addi-

tionally reported that the C-terminal region of GST P1-1 and Hsp72 bound to a C-terminal fragment (200–424) of JNK [7, 15].

The GST P1-1 molecule in the active center consisted of the GSH binding site (G-site) and the substrate binding site (H-site) formed by 38W and 47 C, respectively [19]. As reported previously, GST P1-1 mutants in the active center (W38H and C47S) lacked activity [20, 21]. On the other hand, the positively charged sequence contained residues 194–201 of human GST-pi (especially, 198H and 201R), therefore showing that the C-terminal region of GST P1-1 must bind to the negatively charged C-terminus of JNK (D- and E-rich domain) [7]. Moreover, Adler et al. reported that binding of the C-terminal peptide 194–201 of human GST-pi to the JNK molecule and peptide 34–50 of GST-pi containing the active center region suppressed JNK activity without directly binding to JNK [8, 9].

A recent study revealed that a synthetic conjugate of doxorubicin (DXR) with glutathione (GSH) (GSH-DXR) potently induced apoptosis in rat hepatoma AH66 cells relative to DXR [22–24]. The same study also showed that GSH-DXR inhibited GST activity and suppressed GST P1 mRNA, but DXR did not, indicating that inhibition of the enzyme makes an important contribution to the manifestation of potent GSH-DXR cytotoxicity against AH66 cells [25, 26]. Therefore, it was expected that disappearance of GST P1-1 enzymatic activity did not suppress JNK activity in spite of binding to the JNK molecule and potently inducing apoptosis.

Depending on the cell type, the propagation of the apoptotic death program is expressed in two major ways. Activation of cell-surface death receptors, Fas and tumor necrosis factor receptor-1, leads to the clustering of death domains associated with caspase-8 and to the processing of effector caspases such as caspase-3, -6, and -7 [27–30]. The other caspase cascade, which is known to be activated by genotoxic stresses such as UV irradiation and anticancer drugs, is triggered by cytochrome *c* release from the mitochondria. Moreover, under ER-stress condition, caspase-12 was processed downstream of Apaf-1 and caspase-3 [31]. Released cytochrome *c* binds to the cytoplasmic scaffold, known as Apaf-1, and to procaspase-9, leading to the activation of caspase-9; this in turn activates downstream caspase-3, -6, and -7 [32–36]. It was expected that the activation of JNK induced apoptosis via mitochondria at least.

In the present study, we investigated the molecular interaction between JNK and GST P1-1, which was the mutated active center, and the C-terminal region, and the mechanism of GSH-DXR-induced apoptosis via JNK activation.

Materials and methods

Materials

DXR was obtained from Kyowa Hakko Kogyo (Tokyo, Japan). GSH, 1-chloro-2,4-dinitrobenzene (CDNB), 5-bromo-4-chloro-3-indolyl phosphate and nitro blue tetrazolium tablet (BCIP/NBT) were obtained from Sigma-Aldrich Japan (Tokyo, Japan). Dowex 50W × 8 and glutaraldehyde were purchased from Nakarai Tesque (Kyoto, Japan). Plasmid of pGP5 (rat GST P1 cDNA [37]) was obtained from Health Science Research Resources Bank (Tokyo, Japan).

Acetyl-Asp-Glu-Val-Asp-α-(4-methyl-coumaryl-7-amide) (DEVD-MCA), acetyl-Leu-Glu-His-Asp-α-(4-methyl-coumaryl-7-amide) (LEHD-MCA), LEHD-aldehyde and 7-amino-4-methyl-coumarin (AMC) were purchased from Peptide Institute Inc. (Osaka, Japan). Ex-Taq DNA polymerase and isopropyl β-D-thiogalactopyranoside (IPTG) were purchased from Takara (Tokyo, Japan). Murine anti-human GST-π antibody was purchased from Transduction Laboratories (KY, USA). Vectors of pET3a, pFLAG-CMV4 and pRSET(B) were obtained from Novagen, Sigma-Aldrich Japan and Invitrogen, respectively. Murine anti-His x6 tag antibody and Ni-NTA His-tag bind resin were purchased from Novagen. Rabbit anti-human phospho-c-Jun (63S) antibody and rabbit anti-human phospho-JNK (183T and 185Y) antibody were obtained from Cell Signaling Technology Inc. (MA, USA). All other chemicals were of analytical grade.

Cell lines

The rat ascites hepatoma cell line, AH66, was cultured with RPMI 1640 containing 10% heat inactivated fetal bovine serum (growth medium) under conventional conditions [22–26, 38, 39].

Conjugation of DXR with GSH

GSH-DXR was prepared as described previously [23–26]. In brief, the combination of one mg of each GSH and 0.5 mg of DXR in 0.5 ml of 0.15 M NaCl containing 0.1% glutaraldehyde was incubated at room temperature for 30 min. After incubation, GSH-DXR was separated from GSH and DXR using Dowex 50 W × 8 (H^+ form, 5 × 15 mm). The obtained GSH-DXR was filter-sterilized by a 0.45-μm syringe filter (Corning Coster, Tokyo, Japan). The concentration of DXR was measured by absorbance at 495 nm.

Assay of enzyme activity

GST activity was measured at 340 nm (ε = 9,600) in 1 mM CDNB, 1 mM GSH and 0.1 M sodium phosphate buffer (pH 6.5) at 37°C for 10 min [40].

Caspase-3 and -9 activities were measured in 100 μM of DEVD-MCA and LEHD-MCA, respectively monitored for AMC liberation at 37°C for 15 min in a spectrofluorometer at an excitation/emission wavelength of 380/460 nm, and expressed as pmol AMC per min per mg protein [41].

Construction of the pET3a/mutant GST P1 plasmid

Wild-type GST P1 cDNA inserted into the pET3a vector was prepared by ligation of pET3a and GST P1 cDNA obtained from pGP5 (pET3a/GST P1/wild). A plasmid of the GST P1 deletion mutant of the C-terminal region was constructed by ligation of C-terminal-deleted GST P1 cDNA and pET3a (pET3a/GST P1/ΔC(194–209)). C-terminal (194–209)-deleted GST P1 cDNA with BamHI-site was amplified by PCR using pET3a/GST P1/wild as the template. Plasmids of site-directed mutated GST P1 cDNA, in which the active site residue W38 was replaced with H and the substrate-binding site residue C47 was replaced with S, were prepared and inserted into the pET3a vector (pET3a/GST P1/W38H and pET3a/GST P1/C47S, respectively) as described previously [20, 21]. The plasmid of site-directed mutated GST P1 cDNA in which the C-terminal region 201R was replaced with A was prepared (pET3a/GST P1/R201A) using the Site-directed Mutagenesis Kit (Stratagene, USA).

Expression and purification of recombinant T7-GST P1-1/wild and its mutated T7-GST P1-1 proteins

Plasmids of pET3a/GST P1/wild, pET3a/GST P1/W38H, pET3a/GST P1/C47S, pET3a/GST P1/ΔC(194–209) and pET3a/GST P1/R201A were used for transformation to *E. coli* BL21(DE3) and T7-tagged GST P1-1/wild, GST P1-1/W38H, GST P1-1/C47S, GST P1-1/ΔC(194–209) and GST P1-1/R201A proteins, respectively were expressed by induction with 1mM IPTG. These expressed proteins containing T7-tagged peptide were purified using the T7-tag affinity purification kit (Takara, Tokyo, Japan).

Detection of T7-tagged GST P1-1/wild and its mutant protein (Western blot analysis)

T7-GST P1-1/wild and its mutant proteins were analyzed by Western blotting as previously reported [26]. After immunoreaction using murine anti-T7 antibody (× 1/10,000) as the primary antibody and anti-mouse IgG-alkaline phosphatase conjugate as the secondary antibody (× 1/1,000), GST-P and its mutant bands were visualized with BCIP/NBT.

Construction of pFLAG/mutant GST P1 plasmid and pFLAG/JNK/K55A plasmid

GST P1/wild, GST P1-1/W38H and GST P1-1/C47S cDNAs, prepared from the above-described pET3a plasmids, were inserted into pFLAG-CMV4 (mammalian expression vector). Each of the plasmids obtained was transfected into AH66 cells using the FuGENE 6 transfection reagent (Roche, Japan). The transfectants were selected by treatment with G418.

Wild-type JNK cDNA, which was prepared by RT-PCR using total RNA from AH66 cells as the template, were inserted into the pFLAG-CMV4 vector (pFLAG/JNK/wild). The plasmid of site-directed mutated JNK cDNA, in which the ATP-binding site 55K was replaced with A,was prepared (pFLAG/JNK/K55A) from the resulting pFLAG/JNK/wild as the template using the Site-directed Mutagenesis Kit (Stratagene, USA). This plasmid were transfected into AH66 cells using the FuGENE 6 transfection reagent. The transfectants were selected by treatment with G418. The expressed Flag-JNK/K55A was functioned with JNK dominant negative (JNK-DN).

Preparation of c-Jun fusion resin

The c-Jun cDNA prepared by RT-PCR using total RNA extracted from AH66 cells as the template was ligated to the pRSET(B) vector. The resulting plamid was used for transformation to *E. coli* BL21(DE3) and the recombinant His × 6-tagged c-Jun was expressed by induction with 1 mM IPTG. The expressed protein containing His × 6-tag peptide was absorbed using the NTA-Ni-His-tag resin (Novagen, Tokyo, Japan) and the c-Jun fusion resin was used as the substrate of JNK.

Assay of JNK activity

After treatment of AH66 cells with GSH-DXR for various period of time up to 24 h, JNK was extracted with cell lysis buffer (1% Triton X-100, 20 mM Tris/HCl (pH 7.4), 150 mM NaCl, 0.1 mM Na_3VO_4 and 1 μg/ml leupeptin). JNK activity in the cell extract was measured as follows: JNK was purified from the cell extract by affinity precipitation using c-Jun fusion resin at 4°C overnight. A suspension of JNK-coupled c-Jun fusion resin in kinase buffer (25 mM Tris/HCl (pH 7.5) containing 0.1 mM Na_3VO_4) was incubated with 100 μM ATP at 30°C for 30 min. The eluted phosphorylated c-Jun (His-tagged Pi-c-Jun) and phosphorylated JNK (active form,

Pi-JNK) by imidazole from Ni-NTA resin were analyzed by Western blot analysis using rabbit anti-human phospho-c-Jun (63S) antibody (× 1/1,000) and rabbit anti-human phospho-JNK (183T and 185Y) antibody (× 1/1,000), respectively as the primary antibody. After immunoreaction with anti-rabbit IgG-alkaline phosphatase conjugate as the secondary antibody (× 1/20,000), Pi-c-Jun and Pi-JNK bands were visualized with BCIP/NBT.

T7-GST P1-1 in the mixture (JNK-binding type) was also detected as described above.

Detection of cytochrome *c*

After treatment of AH66 cells with 0.3 μM GSH-DXR, the cells were suspended in hypotonic solution (20 mM HEPES/NaOH (pH 7.4), 10 mM KCl, 1.5 mM $MgCl_2$, 1 mM EDTA, 1 mM dithiothreitol, and 1 mM phenylmethanesulfonyl fluoride). The suspension was centrifuged at 750 × *g* for 10 min, and the resulting supernatant was then centrifuged at 15,000 × *g* for 15 min, followed by collection of both the supernatant (cytosol) and the pellet (mitochondria) fractions [32, 33]. Cytochrome *c* in each fraction suspended in 2% sodium dodecylsulfate was analyzed by Western blot analysis using murine anti-cytochrome *c* antibody (× 1/500) as the primary antibody and anti-mouse IgG-alkaline phosphatase conjugate as the secondary antibody (× 1/1,000); the cytochrome *c* band was visualized with BCIP/NBT.

DNA fragmentation

After treatment of the cells (2×10^6) with GSH-DXR in the presence or absence of 20 μM LEHD-aldehyde, the fragmented DNA was prepared and separated by 2% agarose gel electrophoresis as described previously [26, 42]. The 100-base-pair DNA ladder (Gibco, BRL, N.Y., USA) was used as the standard DNA fragment.

Binding of T7-tagged GST P1-1 and its mutants to JNK and inhibition of JNK activity in the *in vitro* experiment

Activated Pi-JNK was prepared as follows: AH66 cells were irradiated UV at 20W of output for 10 min, cells were then incubated for additional 6 h. After incubation, JNK (containing Pi-JNK) was extracted with cell lysis buffer and purified by c-Jun fusion resin. A suspension of JNK-coupled c-Jun fusion resin in kinase buffer was incubated with or without 10 μg/ml T7-GST-P1-1 or its mutant at 30°C for 30 min, washed with kinase buffer and then incubated with 100 μM ATP in the same buffer at 30°C for 30 min. After reduction with1% 2-mercaptoethanol Pi-c-Jun, Pi-JNK and T7-GST P1-1 or its mutant (JNK-binding type) were analyzed by Western blot analysis as described above.

Protein determination

Protein concentration was assayed by a Bio-Rad protein assay kit using BSA as the standard.

Results

Activation of JNK and apoptosis in AH66 cells treated with GSH-DXR

Due to the significant direct inhibition of GST P1-1 by treatment with the GSH-DXR conjugate, molecular based-interaction between GST P1-1 and the conjugate in apoptosis was highly predictable. To investigate the JNK pathway in GSH-DXR-induced apoptosis, the activity of JNK in AH66 cells treated with GSH-DXR was examined. Treatment of the cells with 0.3 μM GSH-DXR caused a continuous increase in the phosphorylated c-Jun level, reflecting JNK activity up to 6 h after treatment (Fig. 1, Pi-c-Jun). The upper and lower bands showed phosphorylation of two sites (63S and 73S) and one site (63S) in the c-Jun molecule, respectively. The amount of phosphorylated JNK, which is the activated form of JNK, increased in correlation with the activity of JNK in GSH-DXR-treated cells (Fig. 1, Pi-JNK), without any change in the total JNK level in GSH-DXR-treated cells (Fig. 1, JNK). Interestingly, GST P1-1, which co-precipitated with the JNK molecule, showed a slight decrease at 9 and 12 h after treatment with GSH-DXR (Fig. 1, GST P1-1).

As a result of treating the cells with 0.3 μM GSH-DXR, both initiator caspase-9 and effector caspase-3 activities did not increase until 9 h and increased linearly thereafter to

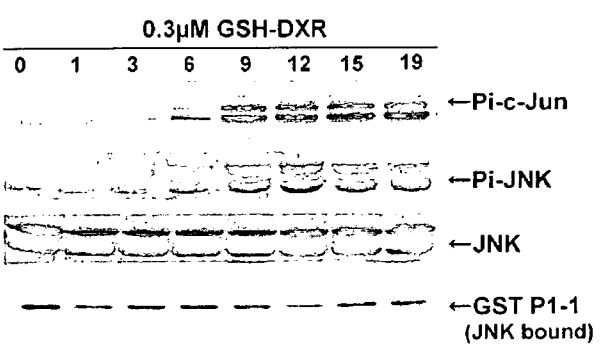

Fig. 1 Activation of JNK by treatment of AH66 cells with 0.3 μM GSH-DXR. Activation of JNK (phosphorylated JNK and phosphorylation of c-Jun), binding of GST P1-1 to the JNK molecule and JNK in AH66 cells treated with 0.3 μM GSH-DXR for various periods of time were measured. Pi-JNK: phosphorylated JNK (active form of JNK), Pi-c-Jun: phosphorylated c-Jun (phosphorylation of c-Jun by active JNK), GST P1-1 (endogenous GST P1-1 bound to the JNK molecule) and JNK (total JNK) were analyzed by Western blot analysis using anti-phospho-JNK (183T and 185Y), anti-phospho-c-Jun (63S), anti-GST-π and anti-JNK antibodies, respectively

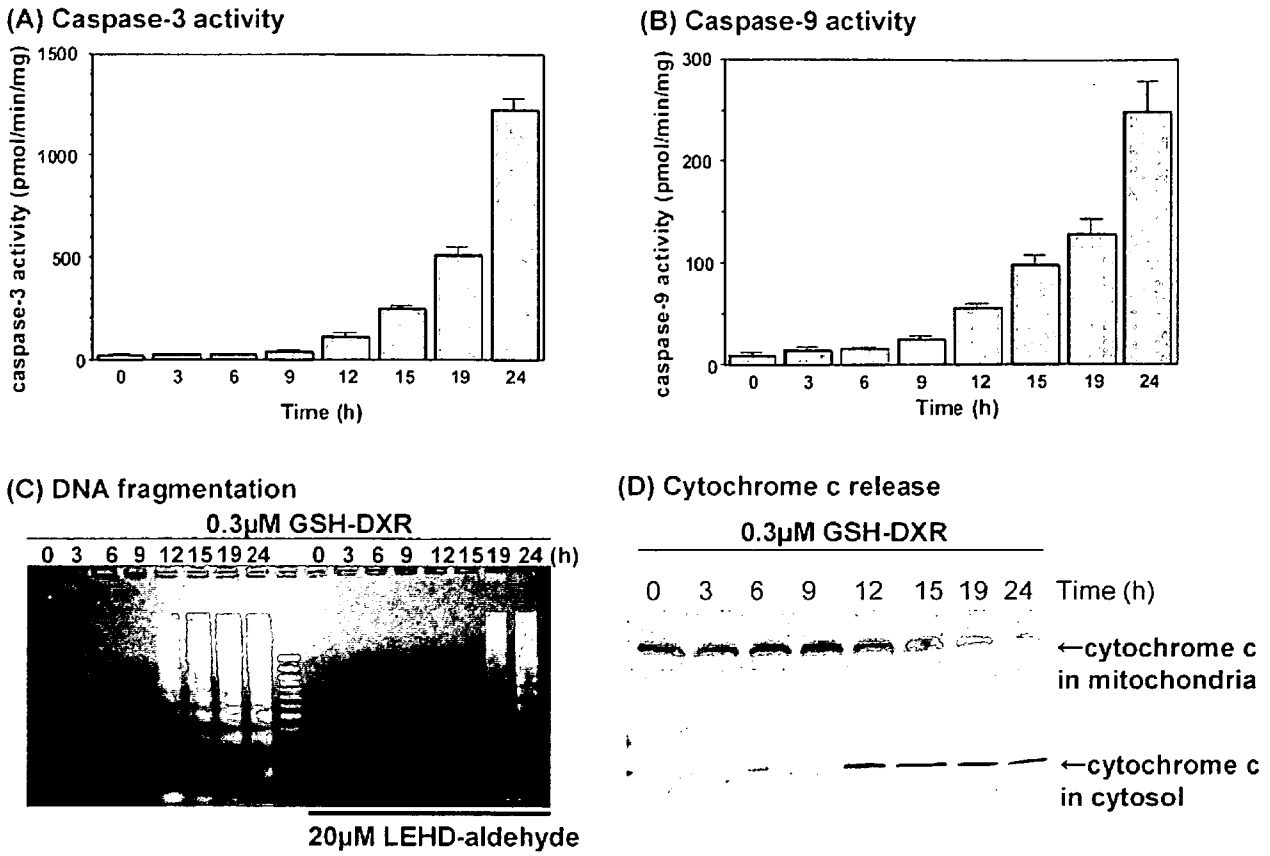

Fig. 2 GSH-DXR (0.3 μM) induced activation of caspase-3, -9, fragmentation of DNA, and release of cytochrome *c* from the mitochondria to cytosol in AH66 cells. Caspase-3 (A) and -9 (B) activation, DNA fragmentation (C), and cytochrome *c* release (D) in AH66 cells treated with 0.3 μM GSH-DXR for various periods of time were measured. DNA fragmentation in AH66 cells co-treated with 0.3 μM GSH-DXR and LEHD-aldehyde (20 μM), caspase-9 inhibitor was also measured. After treatment of AH66 cells with 0.3 μM GSH-DXR for various periods of time, the fragmented DNA was extracted with 1% Triton X-100 and separated by 2% agarose gel electrophoresis. The 100-base-pair DNA ladder (100 bp-Mr, Gibco, BRL, N.Y., USA) was used as the standard DNA fragment. Caspase-3 and -9 activities in the same extracts were determined using DEVD-MCA and LEHD-MCA as substrates. Results are means ± SD (three independent experiments). Cytochrome *c* in both the mitochondrial and cytosolic fractions was detected by Western blot analysis using anti-cytochrome *c* antibody. Amount of applied sample was 100 μg of protein in each lane

a level approximately 60- and 26-fold higher, respectively, than that of the non-treated control at 24 h (Fig. 2(A) and (B)). Under such conditions, DNA fragmentation occurred within 12 h after continuous treatment and the appearance of fragmentation was delayed at 19 h after co-treatment with 20 μM LEHD-aldehyde, which is an inhibitor of caspase-9 (Fig. 2(C)). Moreover, in the mitochondrial pathway in GSH-DXR-induced apoptosis, the release of cytochrome *c* from the mitochondria to cytosol was detected at 12 h after the same treatment (Fig. 2(D)). On the other hand, activation of caspase-8 via the death domain receptor and activation of caspase-12 via ER-stress by treatment with GSH-DXR were measured by enzymatic assay (Ac-IETD-MCA as a substrate, Peptide Inst., Japan) and Western blot analysis using anti-caspase-12 antibody (MBL, Japan), respectively. Caspase-8 was activated by the treatment for 24 h from 35.5 (control) to 788.3 pmol/min/mg, but the cleaved active-form of caspase-12 did not appear (data not shown).

Suppression of GSH-DXR-induced apoptosis by JNK inhibition using JNK inhibitor and JNK-dominant negative (JNK-DN, JNK/K55A)

To confirm the induction of apoptosis by activation of JNK in AH66 cells treated with GSH-DXR, the effect of the JNK activity inhibitor, SP600125, on GSH-DXR-induced DNA fragmentation and activation of caspase-3 and -9 in AH66 cells was measured. Co-treatment of the cells with 5 μM SP600125 suppressed GSH-DXR-induced DNA fragmentation as well as caspase-3 and -9 activation. Furthermore, these activities in the cells treated with 0.3 μM GSH-DXR for 19 h showed decreases from 517.6 to 121.9 pmol/mg/min (caspase-3) and from 187.6 to 51.9 pmol/mg/min (caspase-9) after co-treatment with 5 μM SP600125 (Fig. 3). On the other hand, the effect of JNK/K55A, expression known as JNK-dominant negative (JNK-DN) on GSH-DXR-induced JNK activation and caspase-3 activation (apoptosis induction)

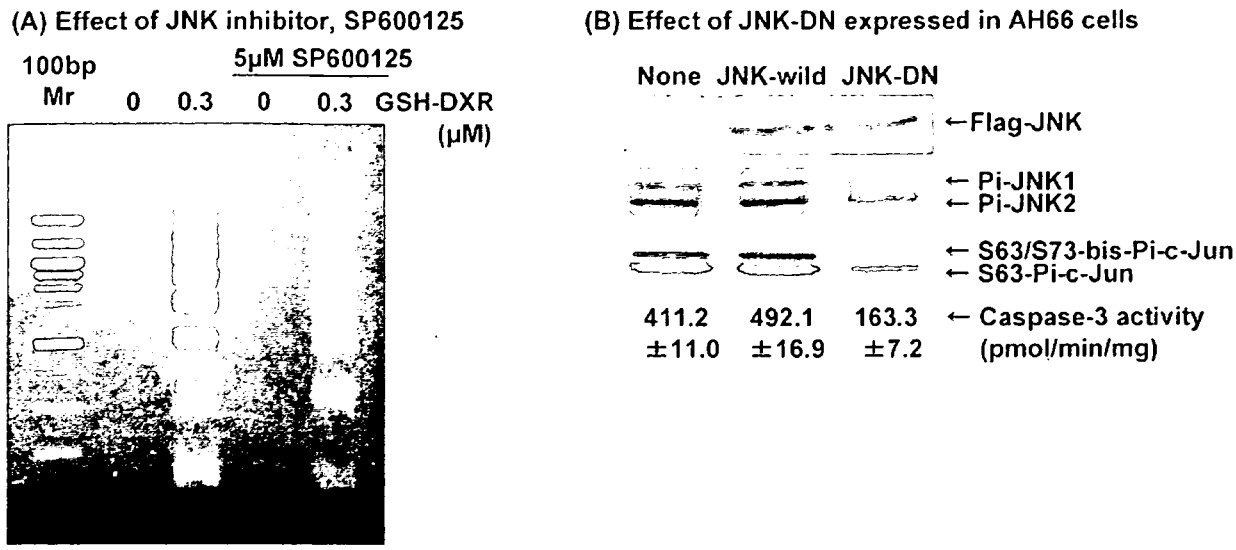

GSH-DXR (μM)	SP600125 (μM)	Activity (pmol/mg/min) Caspase-3	Caspase-9
0	0	5.9 ±1.3	3.5 ±1.1
0.3	0	417.6 ±9.0	187.6 ±6.0
0	5	7.2 ±1.7	5.4 ±1.3
0.3	5	121.9 ±7.9	51.9 ±5.1

Fig. 3 Effect of SP600125 (an inhibitor of JNK activity) (A) and JNK-dominant negative (JNK-DN) (B) on GSH-DXR-induced apoptosis was measured. (A) After co-treatment of AH66 cells with 0.3 μM GSH-DXR and 5 μM SP600125 for 18 h, the fragmented DNA was extracted with 1% Triton X-100 and separated by 2% agarose gel electrophoresis. The 100-base-pair DNA ladder (100 bp-Mr, Gibco, BRL, N.Y., USA) was used as the standard DNA fragment. Caspase-3 and -9 activities in the same extracts were determined using DEVD-MCA and LEHD-MCA as substrates. Results are means ± SD (three independent experiments). (B) After treatment of AH66 cells expressed with Flag-JNK/wild and Flag-JNK/K55A (JNK-DN) with 0.3 μM GSH-DXR for 18 h, activated JNK (Pi-JNK), JNK activity (Pi-c-Jun) and caspase-3 activity were measured. Expressed Flag-tagged JNK was determined by Western blot using anti-Flag antibody. Pi-JNK and Pi-c-Jun were detected with anti-phospho-JNK (183T and 185Y) and anti-phospho-c-Jun (63S) antibodies, respectively

was measured. JNK/K55A, which is a site-directed mutated JNK of the ATP-binding site (K55A), was transfected into AH66 cells. Treatment of the JNK/K55A transfectant with 0.3 μM GSH-DXR resulted in suppression of JNK activation expressed with the phosphorylated c-Jun level compared with that of the JNK/wild transfectant. Caspase-3 activity in the GSH-DXR-treated JNK/K55A transfectant was also decreased in comparison with the same treated JNK/wild transfectant.

GST enzyme activity of T7-GST P1-1 mutants

GST activity of each T7-GST P1-1 mutant was measured using 1mM GSH and 1mM CDNB as substrates (Fig. 4). The enzyme activity of T7-GST P1-1/wild was estimated to be 12.2 μmol/min/mg. T7-GST P1-1/R201A, which was a site-directed mutation of the C-terminal region, maintained activity to the same degree as that of T7-GST P1-1/wild. However T7-GST P1-1/ΔC(194–209), which was a C-terminal deletion mutant, lost activity (under 0.1%

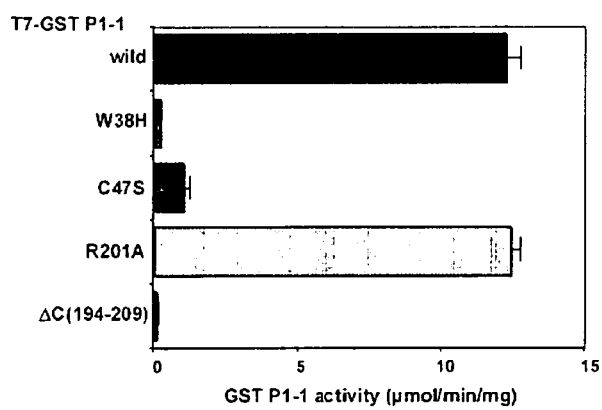

Fig. 4 GST activity in T7-tagged GST P1-1/wild and its mutants (T7-GST P1-1/W38H and T7-GST P1-1/C47S). The activity was determined using 1 mM GSH and 1 mM CDNB as substrates. T7-GST P1-1/wild, T7-tagged wild type GST P1-1; T7-GST P1-1/ΔC(194–209), C-terminal deletion mutant; T7-GST P1-1/R201A, site-directed mutation of the C-terminal region; T7-GST P1-1/W38H and T7-GST P1-1/C47S, site-directed mutation of the active center. Results are means ± SD (three independent experiments)